



Thermal damping
and retardation in
karst conduits

A. J. Luhmann et al.

This discussion paper is/has been under review for the journal Hydrology and Earth System Sciences (HESS). Please refer to the corresponding final paper in HESS if available.

Thermal damping and retardation in karst conduits

A. J. Luhmann¹, M. D. Covington², J. M. Myre², M. Perne^{2,3}, S. W. Jones⁴,
E. C. Alexander Jr.¹, and M. O. Saar^{1,5}

¹University of Minnesota, Department of Earth Sciences, 310 Pillsbury Dr. SE, Minneapolis, Minnesota, 55455, USA

²University of Arkansas, Department of Geosciences, 216 Ozark Hall, Fayetteville, Arkansas, 72701, USA

³Jožef Stefan Institute, Department of Systems and Control, Jamova Cesta 39, Ljubljana, Slovenia

⁴527 Karrow St., Maryville, Tennessee, 37803, USA

⁵ETH-Zürich, Geothermal Energy and Geofluids Group, Department of Earth Sciences, Zürich, Switzerland

Received: 8 July 2014 – Accepted: 2 August 2014 – Published: 13 August 2014

Correspondence to: A. J. Luhmann (luhm0031@umn.edu)

Published by Copernicus Publications on behalf of the European Geosciences Union.

Title Page

Abstract

Introduction

Conclusions

References

Tables

Figures



Back

Close

Full Screen / Esc

Printer-friendly Version

Interactive Discussion



Abstract

Water temperature is a non-conservative tracer in the environment. Variations in recharge temperature are damped and retarded as water moves through an aquifer due to heat exchange between water and rock. However, within karst aquifers, seasonal and short-term fluctuations in recharge temperature are often transmitted over long distances before they are fully damped. Using analytical solutions and numerical simulations, we develop relationships that describe the effect of flow path properties, flow-through time, recharge characteristics, and water and rock physical properties on the damping and retardation of thermal peaks/troughs in karst conduits. Using these relationships, one can estimate the thermal retardation and damping that would occur under given conditions with a given conduit geometry. Ultimately, these relationships can be used with thermal damping and retardation field data to estimate parameters such as conduit diameter. We also examine sets of numerical experiments where we relax some of the assumptions used to develop these relationships, testing the effects of variable diameter, variable velocity, open channels, and recharge shape on thermal damping and retardation to provide some constraints on uncertainty. Finally, we discuss a tracer experiment that provides field confirmation of our relationships. High temporal resolution water temperature data are required to obtain sufficient constraints on the magnitude and timing of thermal peaks and troughs in order to take full advantage of water temperature as a tracer.

1 Introduction

Much of the flow and transport through karst aquifers occurs via conduits (Atkinson, 1977b; Worthington, 1999; Worthington et al., 2000). These preferential flow paths occur in all karst aquifers, but most are poorly characterized or unknown. Hydrogeological investigations of karst aquifers frequently employ hydrographs, chemographs, and thermographs collected from boreholes and springs. Ideally, these data could be used to

HESSD

11, 9589–9642, 2014

Thermal damping and retardation in karst conduits

A. J. Luhmann et al.

[Title Page](#)

[Abstract](#)

[Introduction](#)

[Conclusions](#)

[References](#)

[Tables](#)

[Figures](#)



[Back](#)

[Close](#)

[Full Screen / Esc](#)

[Printer-friendly Version](#)

[Interactive Discussion](#)



provide flow path information, and this characterization would facilitate models that are more capable of predicting flow and transport through these systems.

Hydrographs have been analyzed for more than a century (Boussinesq, 1903, 1904; Maillet, 1905) to characterize flow recession, determine aquifer characteristics, or predict discharge with time (e.g., see summaries in Hall, 1968; Tallaksen, 1995; Jeannin and Sauter, 1998; Dewandel et al., 2003; Ford and Williams, 2007). However, hydrographs provide minimal information about conduit geometry (Covington et al., 2009), and interpretations of karst aquifer structure based on hydrograph analysis are problematic because of the relatively strong control of rainfall frequency on hydrograph shape (Jeannin and Sauter, 1998). Variations in specific conductance often occur with changes in localized recharge (Jakucs, 1959; Newson, 1971; Ternan, 1972; Atkinson, 1977a; Atkinson, 1977b; Worthington et al., 1992; White, 2002). While chemical modification of electrical conductivity signals due to dissolving calcite could theoretically be used to constrain the geometry of flow paths with hydraulic diameters on the mm- to cm-scale, electrical conductivity provides little information about conduits with diameters on the meter-scale and larger, because these larger flow paths produce negligible chemical modification of localized recharge from dissolution (Covington et al., 2012).

Conduits facilitate fast flow-through times and may enable thermal perturbations to reach a spring (e.g., Benderitter et al., 1993; Bundschuh, 1997; Martin and Dean, 1999; Sreaton et al., 2004; Luhmann et al., 2011). These perturbations are modified as water flows through the system, and the modification is sensitive to conduit geometry (Renner, 1996; Liedl et al., 1998; Liedl and Sauter, 1998). The modification occurs because of the heat exchange between water and rock, causing both damping (i.e., decrease in signal amplitude) and retardation (i.e., time lag of the signal) of recharge (Luhmann et al., 2012). Studies have also demonstrated thermal damping and retardation in porous media (e.g., Molson et al., 1992; Palmer et al., 1992; Markle and Schincariol, 2007) and fractures (e.g., Molson et al., 2007). The non-conservative nature of water temperature, even within fairly large conduits, facilitates estimates of conduit size via an analysis of input and output thermographs (Covington et al., 2011;

HESSD

11, 9589–9642, 2014

Thermal damping and retardation in karst conduits

A. J. Luhmann et al.

Title Page

Abstract

Introduction

Conclusions

References

Tables

Figures



Back

Close

Full Screen / Esc

Printer-friendly Version

Interactive Discussion



**Thermal damping
and retardation in
karst conduits**

A. J. Luhmann et al.

[Title Page](#)[Abstract](#)[Introduction](#)[Conclusions](#)[References](#)[Tables](#)[Figures](#)[⏪](#)[⏩](#)[◀](#)[▶](#)[Back](#)[Close](#)[Full Screen / Esc](#)[Printer-friendly Version](#)[Interactive Discussion](#)

Covington et al., 2012; Luhmann et al., 2012; Birk et al., 2014). Unlike chemical modification, the degree of thermal modification depends on the timescale of recharge variations. Shorter, storm-event thermal perturbations provide maximum information about conduits with hydraulic diameters on the meter scale; longer, seasonal thermal perturbations probe smaller, mm- to cm-scale flow paths (Covington et al., 2012). Previous work has also demonstrated that groundwater input into surface streams in karst terrains modifies the relationships between air and water temperatures (O'Driscoll and DeWalle, 2006). The extent of this modification will depend upon whether groundwater has had sufficient residence time to reach thermal equilibration (Luhmann et al., 2011; Covington et al., 2012).

In addition to correlations between thermal signals and conduit geometry, temperature peaks have been used as a simple and inexpensive means to estimate residence times within karst conduit systems when the timing of changes in recharge temperature is known (Martin and Dean, 1999; Birk et al., 2004; Sreaton et al., 2004; Covington et al., 2011). However, since heat exchange within a karst conduit introduces a retardation in the timing of the peak, residence times estimated using temperature will typically be longer than the true residence time. The magnitude of this error, and its functional relationship to conduit geometry and boundary conditions, have not been previously quantified, though Birk et al. (2004) noted that estimates of conduit volume based on temperature lags displayed significantly more scatter than estimates using electrical conductivity lags, and concluded that electrical conductivity provided a more reliable means of estimating travel times.

Recent work used temperature to identify water sources by employing a two component mixing model (Doucette and Peterson, 2014). However, since heat exchange within a karst conduit dampens all thermal perturbations, there will be error in estimates of different water source fractions derived from models that assume conservative endmember temperatures. Temperature mixing models will typically overestimate contributions from background temperature sources and underestimate source waters that provide the thermal perturbations at the thermal peak/trough. Alternatively, during

the thermal recession, the heated or cooled rock surrounding the conduit may potentially facilitate water temperatures that are no longer within the temperature range of the different water sources. The magnitude of these errors will depend upon the extent of water temperature change that occurs along the flow paths.

Our primary objective in this study is to demonstrate the effect of conduit geometry on thermal damping and retardation in karst conduits using both analytical solutions and numerical simulations. We also consider the effects of fluid flow velocity, recharge characteristics, and rock and water physical properties. A relationship between conduit geometry and thermal damping or retardation may ultimately be used to estimate conduit diameter given recharge temperature and down-gradient monitoring data that includes water temperature and a conservative tracer. These relationships can also be used to estimate, and potentially correct for, errors in residence times or water source fractions derived from temperature pulses, and to understand how these errors vary with conduit properties and recharge.

2 Mathematical model

Temperature along a karst conduit as a function of time can be approximated by the 1-D heat advection-dispersion equation:

$$\frac{\partial T_w}{\partial t} = D_L \frac{\partial^2 T_w}{\partial x^2} - V \frac{\partial T_w}{\partial x} + \frac{4h_{\text{conv}}}{\rho_w c_{p,w} D_H} (T_s - T_w), \quad (1)$$

where T_w is the water temperature, t is time, D_L is the longitudinal dispersivity, x is the longitudinal distance down the conduit, V is the water velocity, h_{conv} is the heat transfer coefficient, ρ_w is the density of water, $c_{p,w}$ is the specific heat of water at constant pressure, D_H is the hydraulic diameter of the flow path, and T_s is the conduit wall surface temperature. The terms on the right side of Eq. (1) describe heat dispersion, heat

Thermal damping and retardation in karst conduits

A. J. Luhmann et al.

Title Page

Abstract

Introduction

Conclusions

References

Tables

Figures



Back

Close

Full Screen / Esc

Printer-friendly Version

Interactive Discussion



advection, and heat exchange with the surrounding rock. The convective heat transfer coefficient is given by

$$h_{\text{conv}} = \frac{k_w \text{Nu}}{D_H}, \quad (2)$$

where k_w is the thermal conductivity of water and Nu is the dimensionless Nusselt number, which is the ratio of convective to purely conductive heat transfer through the convective boundary layer near the wall. Nu for turbulent flow is given by the empirically derived Gnielinski correlation (Incropera et al., 2007, Eq. 8.62),

$$\text{Nu} = \frac{(f/8)(\text{Re} - 1000)\text{Pr}}{1 + 12.7(f/8)^{1/2}(\text{Pr}^{2/3} - 1)}, \quad (3)$$

where f is the Darcy–Weisbach friction factor, $\text{Re} = \rho_w V D_H / \mu_w$ is the dimensionless Reynolds number, $\text{Pr} = c_{p,w} \mu_w / k_w$ is the dimensionless Prandtl number of water, and μ_w is the dynamic viscosity of water.

Conduction provides a strong control over heat exchange in karst conduits (Covington et al., 2011). Heat conduction in the rock surrounding a circular conduit with no energy generation can be described, using cylindrical symmetry, by the 2-D heat conduction equation:

$$\frac{1}{r} \frac{\partial}{\partial r} \left(r \frac{\partial T_r}{\partial r} \right) + \frac{\partial^2 T_r}{\partial x^2} = \frac{1}{\alpha_r} \frac{\partial T_r}{\partial t}, \quad (4)$$

where r is the radial distance from the conduit center, T_r is the rock temperature, and $\alpha_r = k_r / (\rho_r c_{p,r})$ is the here-assumed isotropic and homogeneous thermal diffusivity of rock, with k_r denoting the thermal conductivity, ρ_r the density, and $c_{p,r}$ the specific heat. To represent heat transport in rock adjacent to a planar fracture, we use translational symmetry and the heat conduction equation becomes

$$\frac{\partial^2 T_r}{\partial y^2} + \frac{\partial^2 T_r}{\partial x^2} = \frac{1}{\alpha_r} \frac{\partial T_r}{\partial t}, \quad (5)$$

Thermal damping and retardation in karst conduits

A. J. Luhmann et al.

Title Page

Abstract

Introduction

Conclusions

References

Tables

Figures

⏪

⏩

◀

▶

Back

Close

Full Screen / Esc

Printer-friendly Version

Interactive Discussion



where y is the distance from the fracture center.

The boundary conditions are:

$$\left. \frac{\partial T_w}{\partial x} \right|_{x=\text{conduit outlet}} = 0, \quad (6)$$

$$\frac{\partial T_r}{\partial r} \rightarrow 0 \text{ as } r \rightarrow \infty, \quad (7)$$

and

$$k_r \left. \frac{\partial T_r}{\partial r} \right|_{r=\text{conduit wall}} = h_{\text{conv}}(T_s - T_w). \quad (8)$$

In planar coordinates, r in Eqs. (7) and (8) is replaced by y :

$$\frac{\partial T_r}{\partial y} \rightarrow 0 \text{ as } y \rightarrow \infty, \quad (9)$$

$$k_r \left. \frac{\partial T_r}{\partial y} \right|_{y=\text{conduit wall}} = h_{\text{conv}}(T_s - T_w). \quad (10)$$

3 Analytical solutions for damping and thermal retardation

Simplification of Eq. (1) allows derivation of several useful analytical solutions. Karst conduits are frequently advection-dominated, with Peclet Numbers of around 100 (Field and Nash, 1997). Therefore, neglect of longitudinal dispersivity will provide a reasonable approximation in many cases. This approximation will break down for particularly short duration pulses (Hauns et al., 2001), but is more likely to hold for the longer term pulses typically found from natural perturbations. Neglecting longitudinal dispersivity results in

$$\frac{\partial T_w}{\partial t} = -V \frac{\partial T_w}{\partial x} + \frac{4h_{\text{conv}}}{\rho_w c_{p,w} D_H} (T_s - T_w). \quad (11)$$

Title Page

Abstract

Introduction

Conclusions

References

Tables

Figures

⏪

⏩

◀

▶

Back

Close

Full Screen / Esc

Printer-friendly Version

Interactive Discussion



For most relevant cases, where the timescale of the change in water temperature is not extremely short, the approximation $h_{\text{conv}} \rightarrow \infty$ is valid (Covington et al., 2011). In this case heat flow is limited by conduction in the rock, and one obtains a boundary condition

$$T_r(x, y = \text{conduit wall}, t) = T_w(x, t). \quad (12)$$

Heat conduction in the rock along the length of the conduit (the x direction) is neglected, and thus, the equation for heat conduction in the rock becomes

$$\frac{\partial^2 T_r(x, y, t)}{\partial y^2} = \frac{1}{\alpha_r} \frac{\partial T_r(x, y, t)}{\partial t}. \quad (13)$$

3.1 Sinusoidal solution for the planar case

Equations (10) to (13) can be solved for the case of sinusoidally varying water temperature, allowing direct calculation of the thermal damping and retardation of the input wave. The retardation and damping produced for this sinusoidal upstream boundary condition provide significant insight into the response from many pulses found in natural settings, including, as will be seen later, a single isolated pulse. For the sinusoidal solution, we employ a shifted temperature variable defined as

$$T'_r = T_r - T_{r,\infty}, \quad (14)$$

where $T_{r,\infty}$ is the rock temperature at an infinite distance from the conduit axis. For an upstream boundary condition that is sinusoidal in time, the solution for the rock temperature is separable and has the functional form

$$T'_r(x, y, t) = X(x)Y(y)T'_t(t). \quad (15)$$

Since the water and rock temperatures are assumed equal at the boundary (Eq. 12), Eq. (15) contains all of the temperature field. With a sinusoidal upstream boundary condition, the time varying component of the solution is also sinusoidal, $T'_t(t) = T'_{w,\text{in}} e^{-i\omega t}$

Thermal damping and retardation in karst conduits

A. J. Luhmann et al.

Title Page

Abstract

Introduction

Conclusions

References

Tables

Figures

⏪

⏩

◀

▶

Back

Close

Full Screen / Esc

Printer-friendly Version

Interactive Discussion



and $T'_r(x, y, t) = T'_{w,in} X(x) Y(y) e^{-i\omega t}$, where $T'_{w,in}$ is the amplitude of the input temperature variation. Using this in Eq. (13), combined with the boundary condition that $\lim_{y \rightarrow \infty} T'_r = 0$, leads to

$$Y(y) = e^{(-1+i)\sqrt{\frac{\omega}{2\alpha_r}}y}. \quad (16)$$

5 The function $X(x)$, can then be derived using Eqs. (10)–(12) leading to

$$X(x)Y(y)\frac{dT'_t(t)}{dt} = -VY(y)T'_t(t)\frac{dX(x)}{dx} + \frac{4\alpha_r}{\Psi D_H}X(x)T'_t(t)\frac{dY(y)}{dy} \Big|_{y=\text{conduit wall}}, \quad (17)$$

where $\Psi = \rho_w c_{p,w} / (\rho_r c_{p,r})$ is a ratio of the volumetric heat capacities of water and rock. This is an ordinary differential equation with constant coefficients and the solution is an exponential function $X(x) = e^{-\gamma x}$, where

$$10 \quad \gamma = -i\frac{\omega}{V} - (-1+i)\frac{4}{V\Psi D_H}\sqrt{\frac{\alpha_r\omega}{2}}e^{(1-i)\sqrt{\frac{\omega}{2\alpha_r}}y}. \quad (18)$$

For the water temperature at the conduit outlet, $T'_{w,out}$, this gives the solution

$$T'_{w,out}(t) = T'_{w,in} \exp \left[-i\omega t + i\frac{\omega}{V}L + (i-1)\frac{4L}{V\Psi D_H}\sqrt{\frac{\alpha_r\omega}{2}} \right]. \quad (19)$$

Since we are interested only in real solutions, we fix the phase and only look at the real part of the equation.

15 From this solution, one can directly derive both the retardation and damping experienced by each sinusoidal temperature peak. A peak in the output temperature is reached at a distance L (i.e., conduit length) downstream of the input at the time, $t_{\text{peak,out}}$, when the imaginary part of the exponent is zero, that is,

$$-\omega t_{\text{peak,out}} + \frac{\omega}{V}L + \frac{4L}{V\Psi D_H}\sqrt{\frac{\alpha_r\omega}{2}} = 0. \quad (20)$$

The fluid flow-through time through the conduit is $t_{ft} = L/V$, and the retardation of the thermal peak, τ , is the difference

$$\tau = t_{\text{peak,out}} - t_{ft} = \frac{4L}{V\Psi D_H} \sqrt{\frac{\alpha_r}{2\omega}}. \quad (21)$$

As can be seen from the real part of γ , the damping of the upstream temperature peaks observed at the downstream end of the conduit ($x = L$) is given by

$$\frac{T'_{w,\text{out}}}{T'_{w,\text{in}}} = \exp \left[-\frac{4L}{V\Psi D_H} \sqrt{\frac{\alpha_r \omega}{2}} \right]. \quad (22)$$

This solution illustrates a thermal length scale, $\lambda_{T,\text{sin}}$, that is appropriate for sinusoidal temperature variations in the input temperature, with

$$\lambda_{T,\text{sin}} = \frac{V\Psi D_H}{4} \sqrt{\frac{2}{\alpha_r \omega}}. \quad (23)$$

$\lambda_{T,\text{sin}}$ is, to within a dimensionless factor of order one, equivalent to the late time thermal length scale of Eq. (22) in Covington et al. (2012).

3.2 Sinusoidal solution for the cylindrical case

For heat conduction within the rock in the vicinity of a karst conduit with a cylindrical geometry, we again neglect conduction in the direction along the conduit (x) and instead of Eq. (4) we use

$$\frac{\partial^2 T_r(x, r, t)}{\partial r^2} + \frac{1}{r} \frac{\partial T_r(x, r, t)}{\partial r} = \frac{1}{\alpha_r} \frac{\partial T_r(x, r, t)}{\partial t}. \quad (24)$$

The solution remains separable such that

$$T'_r(x, r, t) = X(x)R(r)T'_t(t). \quad (25)$$

Title Page

Abstract

Introduction

Conclusions

References

Tables

Figures

◀

▶

◀

▶

Back

Close

Full Screen / Esc

Printer-friendly Version

Interactive Discussion



Thermal damping and retardation in karst conduits

A. J. Luhmann et al.

Title Page

Abstract

Introduction

Conclusions

References

Tables

Figures

⏪

⏩

◀

▶

Back

Close

Full Screen / Esc

Printer-friendly Version

Interactive Discussion



Again we use sinusoidal $T'_t(t)$ and get $T'_r(x, r, t) = T'_{w,in} X(x) R(r) e^{-i\omega t}$. Substituting this into Eq. (24) gives a Bessel equation whose solutions are Bessel functions. The boundary condition $\lim_{r \rightarrow \infty} R(r) = 0$ limits the solution space to specific linear combinations of Bessel functions that are known as Hankel functions of the first kind, $H_i^{(1)}$. The solution is

$$R(r) = \frac{H_0^{(1)} \left((1+i) \sqrt{\frac{\omega}{2\alpha_r}} r \right)}{H_0^{(1)} \left((1+i) \sqrt{\frac{\omega}{2\alpha_r}} D_H/2 \right)}. \quad (26)$$

As in the planar case, $X(x)$ is obtained from Eq. (11) and has the form $X(x) = e^{-\gamma x}$, where

$$\gamma = -i \frac{\omega}{V} + (i+1) \frac{\sqrt{2\alpha_r \omega} H_1^{(1)} \left((1+i) \sqrt{\frac{\omega}{2\alpha_r}} D_H/2 \right)}{\Psi_{D_H/2} H_0^{(1)} \left((1+i) \sqrt{\frac{\omega}{2\alpha_r}} D_H/2 \right)}. \quad (27)$$

Because of the special functions, this solution is less useful analytically, but provides a straightforward means of calculating the output wave numerically.

4 Numerical integration of the planar case for arbitrary recharge temperature

As shown above, if the temperature at the input is $T_{w,in}(t) = e^{-i\omega t}$ then the temperature at the output is $T_{w,out}(t) = T_{w,in}(t) X(L) = e^{-\gamma(\omega)L - i\omega t}$. A general $T_{w,in}(t)$ can be expressed in terms of its Fourier transform,

$$T_{w,in}(t) = \int_{-\infty}^{\infty} K(\omega) e^{-i\omega t} d\omega, \quad (28)$$

and the output temperature is then calculated as

$$T_{w,out}(t) = \int_{-\infty}^{\infty} K(\omega) e^{-\gamma(\omega)L - i\omega t} d\omega. \quad (29)$$

A Gaussian pulse is of particular interest, since this shape approximates many natural recharge events and is also the functional form we use for the simulations below.

5 We use a Gaussian recharge function of the form

$$T_{w,in}(t) = T_{r,0} + \mathcal{R}_A e^{-\frac{(t-t_{peak,in})^2}{2\sigma^2}}, \quad (30)$$

where $T_{w,in}$ is T_w at $x = 0$, $T_{r,0}$ is the initial rock temperature (or rock temperature at infinity), \mathcal{R}_A is the recharge temperature amplitude, $t_{peak,in}$ is the peak time at $x = 0$, and σ controls the width of the thermal pulse.

10 The Fourier transform is given by

$$K(\omega) = \delta(\omega) + \frac{\mathcal{R}_A C}{\sqrt{2\pi}} e^{-\frac{c^2 \omega^2}{2} + i t_{peak,in} \omega}. \quad (31)$$

Therefore the general solution for a Gaussian pulse can be calculating using the integral

$$T_{w,out}(t) = 1 + \frac{\mathcal{R}_A C}{\sqrt{2\pi}} \int_{-\infty}^{\infty} e^{-\frac{c^2 \omega^2}{2} + i t_{peak,in} \omega} e^{-\frac{L}{\Psi D_H/2} \sqrt{\frac{\alpha_r}{2}} \sqrt{\omega} + i \left(\frac{L}{\Psi D_H/2} \sqrt{\frac{\alpha_r}{2}} \sqrt{\omega} + \left(\frac{1}{V} - t \right) \omega \right)} d\omega. \quad (32)$$

15 In practice, this equation, or Eq. (29) for the general case, must be integrated numerically. However, the Fourier transform solution provides an efficient means of numerically calculating thermographs.

HESSD

11, 9589–9642, 2014

Thermal damping and retardation in karst conduits

A. J. Luhmann et al.

Title Page

Abstract

Introduction

Conclusions

References

Tables

Figures

⏪

⏩

◀

▶

Back

Close

Full Screen / Esc

Printer-friendly Version

Interactive Discussion



5 Numerical simulations

In order to relax the somewhat restrictive assumptions required by the analytical solutions, and particularly to test the applicability of the sinusoidal analytical solutions to the propagation of isolated pulses, we present the results of numerical simulations of thermal pulses. These simulations solve the full version of Eqs. (1) and (4) or (5) for a variety of recharge and flow conditions, conduit geometries, thermal pulse shapes, rock and water physical properties, and also for open channel cases that include radiative heat exchange. For the majority of the simulation set, recharge temperature is varied according to the Gaussian function given in Eq. (30). For each simulation, σ is defined to attain a desired recharge duration, \mathcal{R}_D , or full width at half maximum given by

$$\mathcal{R}_D = 2\sigma\sqrt{2\ln 2}. \quad (33)$$

For the initial condition, T_w and T_r are set equal to T_r at infinity or $T_w(x, t = 0) = T_r(r, t = 0) = 10^\circ\text{C}$.

For most of the simulations, V is constant, although V varies between different simulations. f is approximated for most simulations using the von Kármán Equation,

$$f = [1.74 + 2\log(R/\epsilon)]^{-2}, \quad (34)$$

where $R = D_H/2$ is the conduit radius and ϵ is the roughness height (i.e., the average distance that irregularities on the rock wall protrude into the conduit). We set $\epsilon = 2.15$ cm for all simulations. We also run simulations where f is calculated using the empirical Colebrook-White Equation, and we find that simulation results are identical regardless of the equation used to determine f (Luhmann, 2011).

The finite element package COMSOL Multiphysics[®] (Version 3.5) is used to numerically solve the coupled heat advection-dispersion and conduction equations. Using the Coefficient Form PDE mode in COMSOL, Eq. (1) is solved along a 1-D line, which

HESSD

11, 9589–9642, 2014

Thermal damping and retardation in karst conduits

A. J. Luhmann et al.

Title Page

Abstract

Introduction

Conclusions

References

Tables

Figures

⏪

⏩

◀

▶

Back

Close

Full Screen / Esc

Printer-friendly Version

Interactive Discussion



represents a conduit (Fig. 1a) or fracture (Fig. 1b). Because of axial symmetry, a simulation of conduction in the rock surrounding a circular conduit with full pipe flow may be reduced to a 2-D axisymmetric problem. Thus, Eq. (4) is solved using COMSOL's Conduction Heat Transfer application mode with a 2-D axisymmetric rectangle for cylindrical simulations (Fig. 1a). Similarly, because of translational symmetry across the fracture plane, a simulation of conduction in the rock surrounding a water-filled fracture may be simplified to a 2-D planar problem. Thus, Eq. (5) is solved in a 2-D rectangle in Cartesian coordinates for planar simulations (Fig. 1b). The 1-D line and either the 2-D cylindrical or planar rectangle are coupled to each other at one of the rectangle edges using the Extrusion Coupling Variables feature in COMSOL. The 1-D conduit or fracture line and the rock at the conduit or fracture wall were discretized into 1000 finite elements along the flow path length for all simulations. Mesh resolution gradually coarsens in the 2-D rectangle of rock away from the flow path wall, but the 2-D rectangle was generally discretized into 23 000 elements. COMSOL uses an implicit method to solve the system of equations. User-defined relative and absolute tolerances are compared to the estimated error to modify timestep duration to obtain the desired accuracy. The relative and absolute tolerances were set to $\leq 10^{-6}$ and $\leq 10^{-7}$, respectively.

We conduct numerous simulations where we vary the parameters to consider their effect on thermal damping and retardation. Table 1 lists default values for parameters, but simulations were also run with other values, which are provided in the Supplement. The thermal transmission factor, F , which provides a means to quantify damping, is given by

$$F = \frac{T_{w,\text{peak,out}} - T_{r,\infty}}{T_{w,\text{peak,in}} - T_{r,\infty}}, \quad (35)$$

where $T_{w,\text{peak,out}}$ is the outlet peak water temperature and $T_{w,\text{peak,in}}$ is the inlet peak water temperature. The thermal peak retardation, τ , for each simulation is the time of peak temperature at the outlet minus the flow-through time (Eq. 21). Though the

HESSD

11, 9589–9642, 2014

Thermal damping and retardation in karst conduits

A. J. Luhmann et al.

Title Page

Abstract

Introduction

Conclusions

References

Tables

Figures



Back

Close

Full Screen / Esc

Printer-friendly Version

Interactive Discussion



notation here is in terms of temperature peaks, the same equations apply to temperature troughs. τ and F for all simulations are provided in the Supplement.

6 Results

6.1 Thermal damping

5 The damping of temperature peaks in the simulations shows a dependence on the ratio $L/\lambda_{T,\text{sin}}$. When the ratio $L/\lambda_{T,\text{sin}}$ is small, there is little damping of recharge signals. However, when the ratio $L/\lambda_{T,\text{sin}}$ is large, recharge signals undergo significant to complete damping. For the planar sinusoidal solution, the transmission factor, F , is given by Eq. (22). In order to compare this analytical solution for damping of sinusoids with
 10 the simulations that contain Gaussian input thermographs, we need an approximate conversion between angular frequency of the sinusoid, ω , and an appropriate analog for the Gaussian pulse. We use the relation $\omega = \pi/(C_{\text{time}}\mathcal{R}_D)$, which relates the period of the sinusoid to a multiple of the full width at half maximum of the Gaussian curve. The time conversion constant, C_{time} , is treated as a fitting parameter. Using this approximation, and the definition of the transmission factor (Eq. 35), Eq. (22) can be rewritten as
 15 as

$$F_{\text{planar}} = \exp\left(-\frac{4L}{V\Psi D_H}\sqrt{\frac{\pi\alpha_r}{2C_{\text{time}}\mathcal{R}_D}}\right). \quad (36)$$

For the planar simulations, and cylindrical simulations that are well-approximated with the planar solution, we find that a value of $C_{\text{time}} \approx 4$ provides a tight fit to the transmission factors measured from the pulses in the simulations (Fig. 2). Covington et al.
 20 (2011) showed that the agreement between planar and cylindrical heat transport solutions was dependent on a dimensionless number, $\Theta = (R^2\bar{V})/(L\alpha_r)$, where \bar{V} is a time-averaged or reference flow velocity, with cylindrical cases well-approximated by the

planar solution for $\Theta \gtrsim 10$. Similarly, here we find that Eq. (36) breaks down for cylindrical simulations with small Θ . However, we also find that the error is strongly correlated to Θ , and the damping in the cylindrical cases is well-fit by a correction factor of the form

$$F_{\text{cyl}} = \frac{\Theta}{C_{\text{cyl}} + \Theta} F_{\text{planar}}. \quad (37)$$

This correction factor, with a value of $C_{\text{cyl}} \approx 0.4$, roughly accounts for the additional heat exchange. Though an approximation of the cylindrical solution given in Sect. 3.2 might provide a more well-motivated correction, this equation produces acceptable results and is simpler to implement since it requires no calculation of Hankel functions. Figure 2 shows a comparison between the transmission factors within the simulations and the values of F_{planar} or F_{cyl} for the planar and cylindrical simulations, respectively.

6.2 Thermal retardation

As for thermal damping, the thermal retardation of a Gaussian pulse can be approximated using the form of the sinusoidal solution along with a multiplicative time constant. For thermal retardation, we find that Eq. (21) provides a good approximation to the simulated cases (Fig. 3) with a choice of $\omega \approx \pi/\mathcal{R}_D$, such that

$$\tau_{\text{planar}} = \frac{4L}{V\Psi D_H} \sqrt{\frac{\alpha_r \mathcal{R}_D}{2\pi}}. \quad (38)$$

While this relation provides an excellent fit to the planar cases, and most of the cylindrical cases, cylindrical cases with small values of Θ do produce some scatter. This scatter is sufficiently small that we do not attempt to develop a correction for it. There is also some scatter associated with simulations with relatively slow velocities. This scatter is likely caused by numerical dispersion.

Title Page

Abstract

Introduction

Conclusions

References

Tables

Figures

⏪

⏩

◀

▶

Back

Close

Full Screen / Esc

Printer-friendly Version

Interactive Discussion



6.3 Relaxation of additional assumptions

Our analysis thus far, including the simulations, employs a number of simplifications or approximations, such as constant conduit diameter and constant flow velocity. Here, we run simulations that relax these assumptions to examine potential uncertainty in the F and τ relationships. We consider the effect of variable diameter or flow velocity within an individual conduit and also run open channel simulations, where a conduit is only partially filled with water and radiative heat exchange occurs. Finally, we consider other functions that approximate the shape of recharge thermographs in nature, to examine whether different shapes produce significantly different values of damping or retardation.

6.3.1 Variable hydraulic diameter

The conduit hydraulic diameter, D_H , typically changes along a karst flow path. If this occurs, the thermal signal at the monitoring location of interest will be a composite signal, and estimates of D_H using Eqs. (36) and (38) will then be estimates of an effective hydraulic diameter, $D_{H,e}$, that is some function of the different size flow paths that the water traversed. If the pulse undergoes little modification in shape or duration as it flows through different conduit segments, then the total transmission factor, F_T , in a conduit with multiple segments with different values of D_H , is given by

$$F_T = \prod_{i=1}^n F_i, \quad (39)$$

where F_i is the transmission factor from segment i . Furthermore, the total retardation of the thermal peak, τ_T , is given by

$$\tau_T = \sum_{i=1}^n \tau_i, \quad (40)$$

HESSD

11, 9589–9642, 2014

Thermal damping and retardation in karst conduits

A. J. Luhmann et al.

Title Page

Abstract

Introduction

Conclusions

References

Tables

Figures

⏪

⏩

◀

▶

Back

Close

Full Screen / Esc

Printer-friendly Version

Interactive Discussion



where τ_i is the retardation from segment i . τ_i is given by

$$\tau_i = \left[\frac{4}{\Psi} \sqrt{\frac{\alpha_r \mathcal{R}_D}{2\pi}} \right] \frac{L_i}{V_i D_{H,i}}, \quad (41)$$

where the quantity in square brackets is approximately constant and L_i , V_i , and $D_{H,i}$ are the length, velocity, and hydraulic diameter, respectively, of segment i . It follows that

$$\tau_T = \left[\frac{4}{\Psi} \sqrt{\frac{\alpha_r \mathcal{R}_D}{2\pi}} \right] \sum_{i=1}^n \frac{L_i}{V_i D_{H,i}}. \quad (42)$$

We can define an effective length (L_e), velocity (V_e), and diameter (D_e) such that

$$\tau_T = \left[\frac{4}{\Psi} \sqrt{\frac{\alpha_r \mathcal{R}_D}{2\pi}} \right] \frac{L_e}{V_e D_{H,e}}. \quad (43)$$

From this we can see that, given the quantities in the square bracket are constant, the response of a multi-diameter conduit is the same as that of an equivalent single diameter conduit with the effective length, velocity, and diameter. We can then consider the relationship of $D_{H,e}$ to $D_{H,i}$ as well as the relationship of L_e to L_i . There is more than one equivalent conduit that can be defined depending upon the constraints chosen. We impose the following four constraints, which we deem to be the most physically meaningful:

1. The retardation of the equivalent conduit is equal to that of the multiple segment conduit,

$$\frac{L_e}{V_e D_{H,e}} = \sum_{i=1}^n \frac{L_i}{V_i D_{H,i}}. \quad (44)$$

Thermal damping and retardation in karst conduits

A. J. Luhmann et al.

Title Page

Abstract

Introduction

Conclusions

References

Tables

Figures

◀

▶

◀

▶

Back

Close

Full Screen / Esc

Printer-friendly Version

Interactive Discussion



2. Mass (discharge) is conserved along the multiple segment conduit,

$$V_i D_{H,i}^2 = V_{i+1} D_{H,i+1}^2. \quad (45)$$

3. The multiple segment and equivalent conduits have the same discharge,

$$V_e D_{H,e}^2 = V_i D_{H,i}^2. \quad (46)$$

4. The flow-through time of the multiple segment and equivalent conduits is the same,

$$\frac{L_e}{V_e} = \sum_{i=1}^n \frac{L_i}{V_i}. \quad (47)$$

Using these constraints, it is possible to solve for the equivalent diameter and length,

$$D_{H,e} = \frac{\sum_{i=1}^n L_i D_{H,i}^2}{\sum_{i=1}^n L_i D_{H,i}} = \frac{\text{(Total Conduit Volume)}}{\sum_{i=1}^n (\textit{ith Segment Volume}) / D_{H,i}} = \frac{t_{ft}}{\sum_{i=1}^n t_{ft,i} / D_{H,i}} \quad (48)$$

and

$$L_e = \sum_{i=1}^n \frac{L_i D_{H,i}^2}{D_{H,e}^2} = \frac{\text{(Total Conduit Volume)}}{\text{(Equivalent Conduit Cross Sectional Area)}}. \quad (49)$$

15 The relationships between the equivalent model parameters and conduit volumes or flow-through times assume that the relationship between hydraulic diameter and cross

sectional area is fixed. An analogous derivation using transmission factor, F , rather than retardation, τ , yields the same relationships, and therefore the equivalent models for damping and retardation are the same.

The equivalent diameter is given by the volume- or time-weighted harmonic mean of the hydraulic diameters of the individual segments. Since the harmonic mean accentuates the smaller values in a set, and is always less than the arithmetic mean, one might think that the smaller diameters figure more heavily in the calculation of an equivalent diameter. However, this effect is offset by the weighting by volume, or, equivalently, flow-through time. For the same length, larger diameter conduits will have larger volumes and longer flow-through times. The effect of the weighting is sufficiently strong that, for two conduit segments of equivalent length, the equivalent diameter is more heavily weighted toward the larger diameter.

Since discharge and flow-through time are fixed, the volumes of the multi-segment and equivalent conduits must be the same. Consequently, the length of the equivalent model is equal to this volume divided by the cross-sectional area of the equivalent model conduit. While one might like to hold conduit length fixed between the multi-segment and equivalent models, this is not possible given the constraints (1–4) used above, and we deem these constraints to be more physically meaningful than holding length constant. This is, however, a somewhat arbitrary choice and other equivalent models could also be derived. As an example of the relationship between multiple segment and equivalent conduit properties, Fig. 4 shows the ratio of $D_{H,e}$ to the average hydraulic diameter, $D_{H,avg}$, and the ratio of L_e to $L_1 + L_2$ for systems containing two conduit segments with equal length.

Simulations were run in cylindrical coordinates to test if a conduit with two segments with different diameters and a conduit with a constant effective diameter calculated from Eqs. (48) and (49) produce the same transmission and retardation. We run two example cases of a multiple segment conduit, both of which have two segments with equal lengths and different diameters. In one case D_H increases by 20% halfway down the conduit and in the other case by 100%. Table 2 provides values of model parameters

HESSD

11, 9589–9642, 2014

Thermal damping and retardation in karst conduits

A. J. Luhmann et al.

[Title Page](#)

[Abstract](#)

[Introduction](#)

[Conclusions](#)

[References](#)

[Tables](#)

[Figures](#)

[⏪](#)

[⏩](#)

[◀](#)

[▶](#)

[Back](#)

[Close](#)

[Full Screen / Esc](#)

[Printer-friendly Version](#)

[Interactive Discussion](#)



for each case and the transmission and retardation measured from each simulated thermograph. For the simulations of a conduit with two different D_H segments, the output of the first section was used as input into the second section. For the two example cases, there is good agreement between the transmission factors and retardation observed in the multi-segment and equivalent models (Table 2).

6.3.2 Variable flow velocity

During recharge events, discharge variability causes variations in flow velocity, V . To explore the effect of varying velocity on the amount of damping and retardation that occurs, we ran additional simulations in cylindrical coordinates where velocity was varied and compared them with constant velocity simulations. For each variable velocity simulation, both V and $T_{w,in}$ are defined by a Gaussian equation of the form of Eq. (30). Both curves use the same $t_{peak,in}$ and σ , but the initial velocity, V_0 , and velocity amplitude, V_A , (equivalent to $T_{r,0}$ and \mathcal{R}_A , respectively, in Eq. 30) are both set to 0.1 m s^{-1} for all simulations. This simulates a velocity that ranges from 0.1 to 0.2 m s^{-1} over the duration of the pulse. In these simulations velocity and input temperature began to change at the same time, and the peak water temperature at the input occurs at the same time as the peak velocity in the conduit. Because these are 1-D simulations of full pipe flow, there are no spatial velocity gradients, even though velocity varies as a function of time. We also ran equivalent constant velocity simulations, where the flow velocity for each simulation was set to the average velocity that occurred while the thermal peak was in the conduit during the corresponding variable velocity simulation. Five sets of simulations were run to compare five different recharge duration, \mathcal{R}_D , to flow-through time ratios, L/V .

Table 3 provides transmission and retardation data for simulations that consider the effect of variable velocity. For most cases, each set of variable V and constant V simulations produced similar damping. However, as the ratio of recharge duration to flow-through time decreased, the constant V simulations underwent somewhat more

Thermal damping and retardation in karst conduits

A. J. Luhmann et al.

[Title Page](#)

[Abstract](#)

[Introduction](#)

[Conclusions](#)

[References](#)

[Tables](#)

[Figures](#)



[Back](#)

[Close](#)

[Full Screen / Esc](#)

[Printer-friendly Version](#)

[Interactive Discussion](#)



damping than variable V simulations. In general, thermal retardation values were similar for the constant and variable V simulations. However, thermal peaks from variable V simulations are characterized by more retardation than the constant V cases when $\mathcal{R}_D \lesssim L/V$ and less retardation when $\mathcal{R}_D > L/V$. The fraction of time spent at a velocity above or below the average velocity ultimately controlled whether variable V simulations produced less or more retardation than the corresponding constant V simulation. The maximum difference between thermal retardation observed in the constant and variable V simulations is approximately 30%.

6.3.3 Open channel

If water flows along a conduit with a free surface, then a potentially significant amount of heat exchange occurs via radiation through the air. The significance of this exchange is a function of the time scale of the pulse (Covington et al., 2011). To incorporate radiation, we add one more term to the heat advection-dispersion equation:

$$\frac{\partial T_w}{\partial t} = D_L \frac{\partial^2 T_w}{\partial x^2} - V \frac{\partial T_w}{\partial x} + \frac{4h_{\text{conv}}}{\rho_w c_{p,w} D_H} (T_{s,w} - T_w) + \frac{4h_{\text{rad}} A_d}{\rho_w c_{p,w} D_H A_w} (T_{s,d} - T_w), \quad (50)$$

where $T_{s,w}$ is the wet conduit wall surface temperature, h_{rad} is the radiative heat transfer coefficient, $A_d = P_d/W_{\text{fs}}$ is the ratio of dry conduit perimeter (P_d) to the width of the water's free surface (W_{fs}), $A_w = P_w/W_{\text{fs}}$ is the ratio of wet conduit perimeter (P_w) to W_{fs} , and $T_{s,d}$ is the dry conduit wall surface temperature. h_{rad} is given by

$$h_{\text{rad}} = \frac{\sigma_{\text{SB}}}{A_d} (T_w + T_{s,d}) (T_w^2 + T_{s,d}^2), \quad (51)$$

where $\sigma_{\text{SB}} = 5.67 \times 10^{-8} \text{ W m}^{-2} \text{ K}^{-4}$ is the Stefan–Boltzmann constant. Emissivities of water and rock are close to 1, and temperatures in Eq. (51) are in Kelvin. Finally, the dry perimeter boundary condition is

HESSD

11, 9589–9642, 2014

Thermal damping and retardation in karst conduits

A. J. Luhmann et al.

Title Page

Abstract

Introduction

Conclusions

References

Tables

Figures

⏪

⏩

◀

▶

Back

Close

Full Screen / Esc

Printer-friendly Version

Interactive Discussion



$$k_r \frac{\partial T_{r,d}}{\partial y} \Big|_{y=\text{conduit wall}} = h_{\text{rad}}(T_{s,d} - T_w), \quad (52)$$

where $T_{r,d}$ is the temperature of the dry rock. As before, the wet perimeter boundary condition is given by Eq. (8), where $T_r = T_{r,w}$ (wet rock temperature), $T_s = T_{s,w}$ (wet conduit wall surface temperature), and r becomes y . We ran three sets of simulations with different choices of recharge duration, \mathcal{R}_D , with values equal to 1.67 h, 16.7 h, or 6.9 days. For each set, simulations were run in planar coordinates with conduits that were full, mostly full, half full, and mostly empty. A_w was held constant for all open channel simulations to see how F and τ vary as a function of A_d . All simulations were run with $D_H = 1$ to further facilitate comparisons. Because $\Theta \approx 22$ for all of these planar simulations, they accurately model heat exchange in cylindrical or planar conduits and permit simpler planar simulations (Covington et al., 2011). However, we also ran a simulation with a full conduit in cylindrical coordinates for comparison to planar simulations for each set.

For the range of A_d/A_w ratios and \mathcal{R}_D values considered, there is little difference in the transmission and retardation for each set of simulations with a given recharge duration (Table 4). In general, channels with a free surface undergo slightly more damping than channels that are completely full because there is more rock where heat may be exchanged in the open channel simulations. For the two sets of simulations with longer recharge durations, full planar simulations produce the least retardation, and conduits that are mostly full produce the most retardation.

6.3.4 Thermal recharge shape

Our numerical analysis thus far considers a Gaussian thermal recharge function. This is a rough approximation of the typical shape of thermographs found in natural systems, but natural pulses can display a variety of shapes. To explore the influence of shape on damping and retardation, we run simulations with a variety of other functions that are sometimes used to approximate natural pulses. Table 5 provides thermal

Title Page

Abstract

Introduction

Conclusions

References

Tables

Figures



Back

Close

Full Screen / Esc

Printer-friendly Version

Interactive Discussion



transmission factors and retardation values for two sets of equivalent simulations in cylindrical coordinates. Each set includes a Gaussian function, two types of sine function segments, and a triangular function. Shapes of the recharge thermographs used are shown in Fig. 5. One of the sine-shaped peaks is composed of one period of a sine function from one trough to the next (sine_O) and the other one as half a period between two consecutive zeros of the sine (sine_H). \mathcal{R}_D for Gaussian functions is 6000 s and 60 000 s, respectively. Sine and triangular functions were defined such that the total area under each curve was equal to the respective areas for the Gaussian functions. In both cases, the sine_H curve is the least damped and the triangular thermal recharge is the most damped, although the difference in F between the different recharge functions is small. For the shorter thermal pulse, the Gaussian pulse peaks first, and the triangle, sine_O , and sine_H peaks occur approximately, 4, 4 and 9 % later, respectively, than the Gaussian thermal pulse. For the longer thermal pulse, the triangle pulse peaks approximately 30 % earlier than the Gaussian peak, and the sine_O and sine_H peaks occur approximately 9 and 17 % later, respectively, than the Gaussian peak. There is less damping and more retardation for thermographs that have a wider peak/trough near the peak/trough, except for the triangle pulse with a $\mathcal{R}_D = 6000$ s. However, the triangle pulse is not continuously differentiable, and numerical dispersion likely plays a role.

7 An example field study to test the theory

Luhmann et al. (2012) conducted a field-tracer experiment at Freiheit Spring in south-eastern Minnesota by filling a pool next to a sinkhole, adding tracers, dumping the pool water into the sinkhole, and then monitoring spring breakthrough curves of discharge, temperature, chloride, uranine, delta deuterium, and suspended sediment. The flow path's D_H was estimated by reproducing the damped, retarded thermal signal from the trace with heat transport simulations. We conducted a similar study at the same site three days later. The pool was filled with approximately 12 600 L of water for the later study. The pool water was heated, and 33.02 kg of NaCl were added. Discharge,

HESSD

11, 9589–9642, 2014

Thermal damping and retardation in karst conduits

A. J. Luhmann et al.

Title Page

Abstract

Introduction

Conclusions

References

Tables

Figures



Back

Close

Full Screen / Esc

Printer-friendly Version

Interactive Discussion



**Thermal damping
and retardation in
karst conduits**

A. J. Luhmann et al.

[Title Page](#)[Abstract](#)[Introduction](#)[Conclusions](#)[References](#)[Tables](#)[Figures](#)[Back](#)[Close](#)[Full Screen / Esc](#)[Printer-friendly Version](#)[Interactive Discussion](#)

temperature, electrical conductivity, and suspended sediment data were collected at the spring as the pool water was emptied into the sinkhole. This time, however, the pool was released as two separate pulses. Breakthrough curves are shown in Fig. 6, and all data but suspended sediment time series are provided in Luhmann (2011). Approximately the first half of the 12 600 L of water was released beginning at 16:27 LT on 2 September 2010, and the rest of the pool was emptied into the sinkhole beginning at 16:52 LT.

In general, spring breakthrough curves during this double pulse tracer test displayed similar responses to the single pour tracer experiment three days earlier (see Luhmann et al., 2012 for more discussion about the breakthrough curves from the earlier experiment). Discharge at Freiheit Spring increased shortly after each half of the pool was emptied into the sinkhole, suggesting full pipe flow conditions. Furthermore, the initial changes and peaks in suspended sediment occurred before the initial changes and peaks in conductivity. Finally, initial changes and peaks in temperature occurred later than the initial changes and peaks in conductivity because of temperature's non-conservative behavior.

Because these two field-scale experiments were conducted at the same site three days apart, all parameters that control F and τ except \mathcal{R}_D remained nearly constant. There was some rainfall between the two experiments which caused more background variability in spring parameters before the second study, but hydrodynamic conditions were very similar. Background spring discharges before the first and second traces were 26.7 and 26.8 L s⁻¹, respectively. Additionally, it took 1082 s (Luhmann et al., 2012), 1066, and 1103 s between the pool dump (or partial pool dump) and each respective conductivity/chloride increase at the spring for the first trace, the first pulse of the second trace, and the second pulse of the second trace, respectively. Thus, flow-through time was similar for all three pours, and there was little to no variability in D_H , L , and V between the two experiments. However, \mathcal{R}_D was significantly changed from pour one during the first trace (Luhmann et al., 2012) to pours one and two during the second trace.

We did not collect any robust data at the sinkhole during the pours to provide quantitative \mathcal{R}_D information. However, the time span from the initial increase to the peak in electrical conductivity/chloride at the spring provides a proxy for \mathcal{R}_D during each pour. This took 625 s during the 30 August 2010 experiment (Luhmann et al., 2012) and 502 and 464 s for the first and second pulses, respectively, of the 2 September 2010 experiment. Because τ is proportional to $\mathcal{R}_D^{0.5}$, the thermal retardation of the first or second pulse of the second experiment, $\tau_{\text{Ex}2}$, is given by:

$$\tau_{\text{Ex}2} = \tau_{\text{Ex}1} \frac{\sqrt{\mathcal{R}_{D,\text{Ex}2}}}{\sqrt{\mathcal{R}_{D,\text{Ex}1}}} \quad (53)$$

where $\tau_{\text{Ex}1}$ is the thermal retardation from the first experiment and $\mathcal{R}_{D,\text{Ex}1}$ and $\mathcal{R}_{D,\text{Ex}2}$ are the recharge durations during single and double pulse experiments, respectively. With $\tau_{\text{Ex}1}$ equal to 248 s (Luhmann et al., 2012), the predicted $\tau_{\text{Ex}2}$ for the first and second pulses of the second experiment would be 222 s and 214 s, respectively. In reality, $\tau_{\text{Ex}2}$ was 224 s and 218 s for the first and second pulses of the double pulse experiment, respectively, providing field evidence that $\tau \propto \mathcal{R}_D^{0.5}$.

Samples were not analyzed for chloride during the double pulse tracer test. Thus, our uncertainty in calculating F from either pulse of the double pulse tracer test is larger than our uncertainty from the single pulse tracer test. Therefore, we do not perform a similar calculation with F for the double pulse tracer study. Furthermore, spring water temperature was less stable before the double pulse study, and damping of thermal peaks is less useful when there is more thermal variability in the time preceding the recharge period of interest. For example, during the double pulse study at Freiheit Spring, the second pulse produced a higher temperature peak than the first pulse, even though the second pulse produced a lower conductivity peak with a shorter \mathcal{R}_D (Fig. 6). The heated rock from the first pulse facilitated the propagation of a higher temperature peak during the second pulse. Thus, while the peak temperature from a later pulse is still useful, deriving flow path information from the peak temperature of a later pulse

HESSD

11, 9589–9642, 2014

Thermal damping and retardation in karst conduits

A. J. Luhmann et al.

Title Page

Abstract

Introduction

Conclusions

References

Tables

Figures

⏪

⏩

◀

▶

Back

Close

Full Screen / Esc

Printer-friendly Version

Interactive Discussion



is more complicated than doing so using peak data from an initial pulse that follows a relatively stable background.

The best simulated fit of the temperature breakthrough curve from the single pulse tracer study (Luhmann et al., 2012) occurred with a $D_H = 7$ cm using a heat transport simulation in planar coordinates. The best D_H estimate is 8 cm using τ data from this earlier study and Eq. (38). Similarly, the best D_H estimate is 5 cm using F data from this experiment and Eq. (36).

8 Discussion

8.1 Information content of thermal damping and retardation

Variations in water quantity and quality at karst springs are often used to obtain information about the internal properties of a karst aquifer (e.g., Ashton, 1966; Atkinson, 1977b; Sauter, 1992; Ryan and Meiman, 1996; Birk et al., 2004, 2014; Luhmann et al., 2011; Luhmann et al., 2012; Covington et al., 2012). Specifically, Luhmann et al. (2012) showed that combining breakthrough curves of temperature and conservative tracers allows one to constrain values of flow path diameter. This was achieved by adjusting conduit parameters within a numerical transport simulation to obtain best fitting curves for tracer breakthrough. Here, we illustrate an alternative approach that employs the analytical solution for a sinusoidal recharge temperature. This solution provides a good approximation to the damping and retardation of Gaussian temperature pulses simulated over a wide range of conduit properties and recharge conditions. A single fitting parameter, C_{time} , was used to convert between the time scale of the sinusoidal pulse and the time scale of the Gaussian pulse. The primary advantage of this approach is that it is much easier to estimate a hydraulic diameter from analytical equations that relate to damping or retardation than it is to use a numerical model to try to find the best fitting breakthrough curve. Using the technique presented here, one can extract much

HESSD

11, 9589–9642, 2014

Thermal damping and retardation in karst conduits

A. J. Luhmann et al.

Title Page

Abstract

Introduction

Conclusions

References

Tables

Figures



Back

Close

Full Screen / Esc

Printer-friendly Version

Interactive Discussion



of the information available in the breakthrough curve using one of these two numbers, damping or retardation.

The analytical solution provides explicit relationships for both the transmission (Eq. 36) and retardation (Eq. 38) of a thermal peak as a function of conduit properties (L and D_H), flow velocity, V , recharge duration, \mathcal{R}_D , and quantities that are related to the thermal properties of water and rock (Ψ and α_r). The thermal properties of water and rock are relatively constant within a given aquifer, and even do not vary that substantially among near-surface karst aquifers. While an estimate of these parameters is needed to relate damping and retardation to conduit properties, once an estimate is made we typically can treat these as constants for a given site. The conduit length and velocity only occur in Eqs. (36) and (38) as a ratio, L/V , which is equal to the flow-through time, t_{ft} . Therefore, we can reduce these two parameters to a single parameter that is also physically meaningful and more easily measured in the field. This leaves three variables, t_{ft} , \mathcal{R}_D , and D_H , that relate to the damping and retardation via two equations. Therefore, if both damping and retardation are measured at a field site, then we have two equations and three unknowns. One might expect that only one of these three unknowns would need to be constrained by additional field data, and then the other two could be calculated from the relations. However, the relations for damping and retardation are not entirely linearly independent, and therefore contain some duplicate information.

A Maclaurin Series expansion of the exponential in Eq. (36) shows that for low to moderate amounts of damping the transmission factor, F , scales roughly as

$$(1 - F) \propto \frac{t_{ft}}{D_H \mathcal{R}_D^{0.5}}. \quad (54)$$

Regardless of the extent of damping, the retardation scales as

$$\tau \propto \frac{t_{ft} \mathcal{R}_D^{0.5}}{D_H}. \quad (55)$$

HESSD

11, 9589–9642, 2014

Thermal damping and retardation in karst conduits

A. J. Luhmann et al.

Title Page

Abstract

Introduction

Conclusions

References

Tables

Figures

⏪

⏩

◀

▶

Back

Close

Full Screen / Esc

Printer-friendly Version

Interactive Discussion



Since t_{ft} and D_H enter both relations in the same combination, one of these two variables must be constrained from data in order to solve for the other variables. This conclusion only holds for the low damping regime, but this is also the regime in which damping or retardation could feasibly be measured in the field.

5 These considerations about the independence of the damping and retardation equations are largely theoretical. In real world cases, both t_{ft} and \mathcal{R}_D are relatively easy to measure, and it is more likely that both of these will be measured and then used to make separate estimates of D_H using both the damping and retardation equations. If these duplicate estimates are substantially different from each other, then it would
10 suggest that some assumptions of the model are being broken or that one or more of the measurements was in error.

Thermal damping and retardation are not affected by the recharge amplitude (\mathcal{R}_A) or the thermal conductivity (k_w) or dynamic viscosity of water (μ_w). However, it may be impossible to determine F and τ information if \mathcal{R}_A is small. Thus, recharge temperatures that are further from background temperatures make it more practical to use
15 water temperature as a tracer to potentially provide flow path information.

8.2 Limitations of the model

A fairly large number of simplifying assumptions separate the analytical solution presented above from a natural karst conduit. Therefore, it is worth considering the likely
20 effects of these assumptions, and the extent to which the solution will fail in different settings. Among the assumptions behind the analytical solution are: (1) a sinusoidal recharge temperature, (2) a single conduit diameter, (3) no longitudinal dispersion, (4) constant discharge, and (5) rock and water thermal properties that are constant throughout the system.

25 While seasonal temperature variations might be well represented by a sinusoidal solution, most temperature variations at karst springs come in the form of short peaks due to recharge events. However, the numerical simulations presented above demonstrate that, with the help of a fitting parameter, the sinusoidal solution for damping and

Thermal damping and retardation in karst conduits

A. J. Luhmann et al.

[Title Page](#)

[Abstract](#)

[Introduction](#)

[Conclusions](#)

[References](#)

[Tables](#)

[Figures](#)



[Back](#)

[Close](#)

[Full Screen / Esc](#)

[Printer-friendly Version](#)

[Interactive Discussion](#)



retardation can be applied to a variety of single-peak functions, including Gaussians, a triangle pulse, and sine peaks. This may not be the case for multipeak functions, particularly if the peaks are more closely spaced than those of the sinusoidal function. In that case, earlier peaks will likely influence the behavior of later peaks.

5 The analytical solution allows estimation of a single conduit diameter, whereas karst conduits can display a substantial variation in diameter along their length. Therefore a key question is how this estimated diameter is related to the physical conduit properties. The estimated diameter is the diameter of an equivalent conduit that produces the same thermal damping and retardation. It is possible to derive more than one equivalent model depending upon the constraints and assumptions applied. However, for
10 a seemingly reasonable set of constraints the effective diameter is the flow-through time weighted harmonic mean of the hydraulic diameter of the real conduit. To derive this equivalent model, it was assumed that the thermograph time scale does not substantially change as it passes through the system. For the two example simulation sets,
15 the equivalent diameter, so defined, produces the same transmission and retardation as a multi-segment conduit with different diameters (Sect. 6.3.1). This provides some verification that the approach is reasonable, though the approximation is likely to break down for cases where the flow-through time is much longer than the pulse duration. However, this is also the limit in which pulses will be substantially damped and difficult
20 or impossible to observe.

Rather than consisting of a single flow path, natural karst conduits typically contain a network of flow paths of various sizes. Branchwork patterns are quite common, but a variety of network topologies are possible. Physical interpretation of thermal damping and retardation is most straightforward when the system is dominated by a single
25 flow path, such as a sink-rise system. In this case, estimates of conduit diameter apply to the primary conduit. However, thermal tracing experiments between injection points and a spring, as conducted by Luhmann et al. (2012), may also allow characterization of conduit diameters along the flow path between those two points. It is less clear how to interpret natural temperature pulses at a spring fed by a branchwork system, since

HESSD

11, 9589–9642, 2014

Thermal damping and retardation in karst conduits

A. J. Luhmann et al.

Title Page

Abstract

Introduction

Conclusions

References

Tables

Figures



Back

Close

Full Screen / Esc

Printer-friendly Version

Interactive Discussion



water arriving at the spring will have flowed via a large number of different paths of different lengths and diameters. In such cases, network properties are likely to play a significant role, and a better understanding of heat transport within networks is required.

The analytical solution also assumes that longitudinal dispersion can be neglected. While karst conduits tend to have high Peclet numbers, and therefore be advection-dominated, dispersion is certain to play a role for increasingly short duration pulses. Therefore care is needed when applying this solution to short injection pulses, particularly if they propagate a substantial distance. However, the tracer pulses described in Sect. 7 are relatively short, and still display the scaling predicted by the theory. In that case, the flow path was also short, which may minimize the influence of dispersion. In addition to longitudinal dispersion, immobile fluid regions such as pools and eddys can substantially influence tracer behavior (Field and Pinsky, 2000). Again, such effects are likely to be largest for short-duration pulses.

The solution assumes constant discharge in time and with distance along the conduit. In Sect. 6.3.2, we use simulations to explore the effect of varying discharge in time. We find that discharge variability has a relatively modest effect on damping and retardation, and that the direction of the effect is dependent upon the relative magnitude of the flow-through time and recharge duration. Addition of water along the conduit may also have a substantial effect. If the main conduit flow is diluted by water recharged through more diffuse (e.g., matrix or fracture) flow paths, then that water will cause additional damping of the pulse. A gradual addition of matrix water can also influence the retardation, albeit less substantially. Further simulations and field experiments could better quantify the effects of dilution and mixing.

Finally, the thermal properties of rock and water are assumed to be constant throughout the aquifer. While the thermal properties of carbonate rocks within karst aquifers can be somewhat variable (Beardsmore and Cull, 2001), uncertainty can be reduced if measured thermal properties for specific formations of interest are available. However, there are still some potential limitations. In particular, many karst conduits contain

Thermal damping and retardation in karst conduits

A. J. Luhmann et al.

[Title Page](#)

[Abstract](#)

[Introduction](#)

[Conclusions](#)

[References](#)

[Tables](#)

[Figures](#)



[Back](#)

[Close](#)

[Full Screen / Esc](#)

[Printer-friendly Version](#)

[Interactive Discussion](#)



a substantial layer of sediments on the floor. The heat transfer properties of such sediments are likely to be more variable than that of the solid rock at the field site of interest, and in some cases hyporheic exchange is likely to play an important role.

8.3 Considerations for field studies

5 Determination of the damping and retardation of a thermal peak requires high resolution data for both temperature and a conservative tracer in order to capture sharp features in the data. In some cases, data output intervals may need to be on the order of seconds to provide sufficient constraints on the timing and magnitude of thermal peaks/troughs. Due to memory or power limitations, data are not often collected at
10 such a high frequency. Consequently, deploying loggers with the capacity to modify data output intervals based on real-time monitoring, or with the capability to transfer data remotely in real time, may be particularly useful.

Monitoring installations in karst frequently have equipment to record water level, electrical conductivity, and temperature. In general, water level data has little use in
15 determining retardation, since initial hydrograph perturbations often record arrival of pre-event water. Even in the case of open channel conduits, the discharge pulse, which travels as a kinematic wave, will arrive before the event water. In contrast, spring electrical conductivity perturbations can record event water arrival (e.g., Raeisi et al., 2007), and electrical conductivity interacts more slowly with the rock surrounding a conduit
20 than temperature (Birk et al., 2006; Covington et al., 2012). Thus, in many cases, retardation may be estimated as the time difference between the electrical conductivity and temperature peaks or troughs.

Determining the damping of a thermal peak requires an estimate of recharge temperature, in addition to a thermograph at the spring. In some cases, recharge temperature
25 can be monitored at an upstream monitoring location. If this is not possible, recharge temperature may also be approximated in some special cases, such as during a snowmelt event. Dilution can also have a strong effect on damping, and therefore

Thermal damping and retardation in karst conduits

A. J. Luhmann et al.

Title Page

Abstract

Introduction

Conclusions

References

Tables

Figures



Back

Close

Full Screen / Esc

Printer-friendly Version

Interactive Discussion



an estimate of dilution is needed, for example by measuring flow at the recharge and discharge points.

While it can be relatively easy to determine thermal retardation using electrical conductivity and temperature data at some monitoring location of interest, interpretation of thermal damping and retardation is most easily accomplished in systems that contain a sinking surface stream. The values of thermal damping and retardation can be estimated during periods of relatively constant discharge between precipitation events. While flow-through time remains relatively constant during these periods, oscillations in surface stream recharge temperature will cause diurnal thermal oscillations at a downstream monitoring location, so long as heat exchange along the conduit is sufficiently ineffective (Luhmann et al., 2011). Measuring discharge at both upstream and downstream monitoring locations allows an estimate of the degree of dilution that occurs along the flow path to facilitate determination of F and constrain potential uncertainty in the measurement of τ and F . Injection of a conservative tracer permits estimates of flow-through time, and thus facilitates calculation of τ when used in conjunction with the travel time of diurnal thermal peaks or troughs from the upstream to the downstream monitoring locations. Measurements of damping and retardation in a sink-rise system are more difficult to obtain during natural recharge events, since temperature and recharge rates may vary independently, and flow-through time will also vary throughout the event. However, simultaneous monitoring of conductivity and temperature at the recharge and discharge points, particularly if combined with recharge and discharge hydrographs, may still enable measurement of damping and retardation in many settings. In addition to sink-rise systems, interpretation of damping and retardation may be relatively straightforward during tracer studies with a known recharge input. In this case, the more heavily the system is perturbed, the easier it will be to interpret the results.

If recharge can be monitored, then \mathcal{R}_D is given by the full width at half maximum of the recharge thermograph (Eq. 33). The actual shape of the pulse will ultimately be a source of uncertainty. When recharge cannot be monitored, a related time scale to

HESSD

11, 9589–9642, 2014

Thermal damping and retardation in karst conduits

A. J. Luhmann et al.

Title Page

Abstract

Introduction

Conclusions

References

Tables

Figures



Back

Close

Full Screen / Esc

Printer-friendly Version

Interactive Discussion



the \mathcal{R}_D is given by the time from the initial change to the peak/trough in a chemograph during a recharge event, as we did in Sect. 7. If necessary, the time from the initial change to the peak/trough in a thermograph may be used, although the thermograph will not be as accurate since the pulse is modified.

Both thermal damping and retardation data can potentially be used to estimate the hydraulic diameter of a karst conduit. However, measurement of retardation, rather than damping, has inherent advantages. There is better agreement in τ between analytical solutions and numerical simulations than there is with F . This suggests that estimates of D_H may have less uncertainty when using τ values. Furthermore, it is easier to determine τ in the field than F , since estimates of τ only require temperature and electrical conductivity data at the monitoring location of interest, whereas estimates of F also require information about recharge into the system. Finally, damping is more severely impacted by any dilute inflow occurring along the flow path.

9 Conclusions

As water flows through an aquifer, heat exchange occurs between water and rock if they are in thermal disequilibrium. When thermal equilibrium is not attained, the water-rock interaction produces a damped thermal signal in the water that is retarded behind the actual groundwater velocity. Our analytical derivations and numerical simulations demonstrate that the damping and retardation of thermal peaks in conduits or fractures depend on the flow path's hydraulic diameter, flow-through time, and the timescale of the temperature variation. Damping and retardation are also dependent on rock thermal conductivity, k_r , rock specific heat, $c_{p,r}$, rock density, ρ_r , water specific heat, $c_{p,w}$, and water density, ρ_w . However, these parameters vary relatively little within shallow aquifers. Because of this, the relationships for damping and retardation developed here may be used to estimate the hydraulic diameter of a flow path given estimates of the flow-through time and the timescale of temperature variations. Our tracer studies at Freiheit Spring provide some evidence for the applicability of these relationships.

Thermal damping and retardation in karst conduits

A. J. Luhmann et al.

Title Page

Abstract

Introduction

Conclusions

References

Tables

Figures



Back

Close

Full Screen / Esc

Printer-friendly Version

Interactive Discussion



Additional field work is needed to test the usefulness of these relationships when working with more complex flow paths found in nature.

Simulations with variable D_H or V , open channels, and sine- or triangular-shaped thermograph shapes produce some variability in F and τ when compared to simulations with constant D_H or V , full pipe flow, and Gaussian-shaped thermographs. However, variability is generally small, and uncertainty from these conditions should not prevent estimates of D_H using F and τ . In general, estimates of D_H from natural conduits with variable D_H represent a flow-through time weighted harmonic mean of D_H . The effect of variable V on F and τ relationships is more complex, and additional work is necessary to further understand the effect of the shape and timing of different velocity functions on spring thermographs. Finally, the difference in F and τ between conduits with or without free water surfaces depends on the time scale of temperature variation, but open channels will produce somewhat more damping and retardation than conduits that are water-filled.

Luhmann et al. (2012) conducted a field tracer experiment that involved temperature, conductivity/chloride, and other parameters. They were able to estimate a flow path's D_H using known recharge data, high resolution output data, and heat transport simulations which reproduced the damped, retarded thermal signal that resulted from the trace. The dependence of F and τ on D_H derived here enables a new technique. Specifically, one may estimate the conduit diameter using observations of only the damping and retardation of thermal pulses from natural recharge events or tracer experiments. There is likely more error in D_H estimates using this new technique. However, it allows extraction of much of the information carried by the thermal pulses with the ease of employing an analytical solution.

The Supplement related to this article is available online at doi:10.5194/hessd-11-9589-2014-supplement.

HESSD

11, 9589–9642, 2014

Thermal damping and retardation in karst conduits

A. J. Luhmann et al.

Title Page

Abstract

Introduction

Conclusions

References

Tables

Figures

⏪

⏩

◀

▶

Back

Close

Full Screen / Esc

Printer-friendly Version

Interactive Discussion



**Thermal damping
and retardation in
karst conduits**

A. J. Luhmann et al.

[Title Page](#)[Abstract](#)[Introduction](#)[Conclusions](#)[References](#)[Tables](#)[Figures](#)[Back](#)[Close](#)[Full Screen / Esc](#)[Printer-friendly Version](#)[Interactive Discussion](#)

Acknowledgements. A. J. Luhmann was supported by a Doctoral Dissertation Fellowship from the University of Minnesota Graduate School. J. M. Myre was supported by the National Science Foundation (NSF) through an Earth Sciences Postdoctoral Fellowship (EAR-1249895). M. O. Saar acknowledges the NSF under Grant EAR-0941666. Any opinions, findings, and conclusions or recommendations expressed in this material are those of the authors and do not necessarily reflect the views of the NSF. M. O. Saar also thanks the ETH-Zürich for its endowment support of the Geothermal Energy and Geofluids Group as well as the George and Orpha Gibson Endowment for its support of the Hydrogeology and Geofluids Group in the Department of Earth Sciences at the University of Minnesota. Funding for the pool trace study at Freiheit Spring was provided by the Minnesota Environment and Natural Resources Trust Fund as recommended by the Legislative-Citizen Commission on Minnesota Resources (LCCMR). We thank Susan, Aaron, and Matt Kolling for access to their property at Freiheit Spring, and Greg Brick, Su Yi Chai, Dwight Luhmann, and Peter Putzier for assistance with the pool trace study.

References

- Ashton, K.: The analysis of flow data from karst drainage systems, *The Transactions of the Cave Research Group*, 7, 161–203, 1966. 9615
- Atkinson, T. C.: Carbon dioxide in the atmosphere of the unsaturated zone: An important control of groundwater hardness in limestones, *J. Hydrol.*, 35, 111–123, 1977a. 9591
- Atkinson, T. C.: Diffuse flow and conduit flow in limestone terrain in the Mendip Hills, Somerset (Great Britain), *J. Hydrol.*, 35, 93–110, 1977b. 9590, 9591, 9615
- Beardsmore, G. R. and Cull, J. P.: *Crustal Heat Flow: A Guide to Measurement and Modelling*, Cambridge University Press, Cambridge, UK, 2001. 9619
- Benderitter, Y., Roy, B., and Tabbagh, A.: Flow characterization through heat transfer evidence in a carbonate fractured medium: first approach, *Water Resour. Res.*, 29, 3741–3747, 1993. 9591
- Birk, S., Liedl, R., and Sauter, M.: Identification of localised recharge and conduit flow by combined analysis of hydraulic and physico-chemical spring responses (Urenbrunnen, SW-Germany), *J. Hydrol.*, 286, 179–193, 2004. 9592, 9615

**Thermal damping
and retardation in
karst conduits**

A. J. Luhmann et al.

[Title Page](#)[Abstract](#)[Introduction](#)[Conclusions](#)[References](#)[Tables](#)[Figures](#)[⏪](#)[⏩](#)[◀](#)[▶](#)[Back](#)[Close](#)[Full Screen / Esc](#)[Printer-friendly Version](#)[Interactive Discussion](#)

- Birk, S., Liedl, R., and Sauter, M.: Karst spring responses examined by process-based modeling, *Ground Water*, 44, 832–836, 2006. 9620
- Birk, S., Wagner, T., and Mayaud, C.: Threshold behavior of karst aquifers: the example of the Lurbach karst system (Austria), *Environ. Earth Sci.*, doi:10.1007/s12665-014-3122-z, in press, 2014. 9592, 9615
- 5 Boussinesq, J.: Sur un mode simple d'écoulement des nappes d'eau d'infiltration à lit horizontal, avec rebord vertical tout autour lorsqu'une partie de ce rebord est enlevée depuis la surface jusqu'au fond, *CR Acad. Sci.*, 137, 5–11, 1903. 9591
- Boussinesq, J.: Recherches théoriques sur l'écoulement des nappes d'eau infiltrées dans le sol et sur le débit des sources, *J. Math. Pure. Appl.*, 10, 5–78, 1904. 9591
- 10 Bundschuh, J.: Temporal variations of spring water temperatures in relation to the extents of heat transport modes occurring in the karstified lower Gypsum-Keuper aquifer (Karnian, southern Germany), in: *Proceedings of the 12th International Congress of Speleology, 6th Conference on Limestone Hydrology and Fissured Media, 10–17 August 1997, La Chaux de Fonds, Switzerland, vol. 2, 129–132, 1997. 9591*
- 15 Covington, M. D., Wicks, C. M., and Saar, M. O.: A dimensionless number describing the effects of recharge and geometry on discharge from simple karstic aquifers, *Water Resour. Res.*, 45, W11410, doi:10.1029/2009WR008004, 2009. 9591
- Covington, M. D., Luhmann, A. J., Gabrovšek, F., Saar, M. O., and Wicks, C. M.: Mechanisms of heat exchange between water and rock in karst conduits, *Water Resour. Res.*, 47, W10514, doi:10.1029/2011WR010683, 2011. 9591, 9592, 9594, 9596, 9603, 9610, 9611
- 20 Covington, M. D., Luhmann, A. J., Wicks, C. M., and Saar, M. O.: Process length scales and longitudinal damping in karst conduits, *J. Geophys. Res.-Earth*, 117, F01025, doi:10.1029/2011JF002212, 2012. 9591, 9592, 9598, 9615, 9620
- 25 Dewandel, B., Lachassagne, P., Bakalowicz, M., Weng, P., and Al-Malki, A.: Evaluation of aquifer thickness by analysing recession hydrographs. Application to the Oman ophiolite hard-rock aquifer, *J. Hydrol.*, 274, 248–269, 2003. 9591
- Doucette, R. and Peterson, E. W.: Identifying water sources in a karst aquifer using thermal signatures, *Environ. Earth Sci.*, doi:10.1007/s12665-014-3387-2, in press, 2014. 9592
- 30 Field, M. S. and Nash, S. G.: Risk assessment methodology for karst aquifers: (1) Estimating karst conduit-flow parameters, *Environ. Monit. Assess.*, 47, 1–21, 1997. 9595
- Field, M. S. and Pinsky, P. F.: A two-region nonequilibrium model for solute transport in solution conduits in karstic aquifers, *J. Contam. Hydrol.*, 44, 329–351, 2000. 9619

Thermal damping and retardation in karst conduits

A. J. Luhmann et al.

[Title Page](#)

[Abstract](#)

[Introduction](#)

[Conclusions](#)

[References](#)

[Tables](#)

[Figures](#)

[⏪](#)

[⏩](#)

[◀](#)

[▶](#)

[Back](#)

[Close](#)

[Full Screen / Esc](#)

[Printer-friendly Version](#)

[Interactive Discussion](#)



- Ford, D. C. and Williams, P.: Karst Hydrogeology and Geomorphology, John Wiley & Sons, Chichester, England, 2007. 9591
- Hall, F. R.: Base-flow recessions – a review, *Water Resour. Res.*, 4, 973–983, 1968. 9591
- Hauns, M., Jeannin, P.-Y., and Atteia, O.: Dispersion, retardation and scale effect in tracer breakthrough curves in karst conduits, *J. Hydrol.*, 241, 177–193, 2001. 9595
- Incropera, F. P., DeWitt, D. P., Bergman, T. L., and Lavine, A. S.: *Fundamentals of Heat and Mass Transfer*, 6th Edn., John Wiley & Sons, Hoboken, New Jersey, USA, 2007. 9594
- Jakucs, L.: Neue methoden der höhlenforschung in Ungarn und ihre ergebnisse, *Die Höhle*, 10, 88–98, 1959. 9591
- Jeannin, P.-Y. and Sauter, M.: Analysis of karst hydrodynamic behaviour using global approaches: A review, *Bulletin d'Hydrogéologie*, 16, 31–48, 1998. 9591
- Liedl, R. and Sauter, M.: Modelling of aquifer genesis and heat transport in karst systems, *Bulletin d'Hydrogéologie*, 16, 185–200, 1998. 9591
- Liedl, R., Renner, S., and Sauter, M.: Obtaining information about fracture geometry from heat flow data in karst systems, *Bulletin d'Hydrogéologie*, 16, 143–153, 1998. 9591
- Luhmann, A. J.: *Water Temperature as a Tracer in Karst Aquifers*, Ph.D. thesis, available at: <http://purl.umn.edu/113204>, University of Minnesota, Minneapolis, Minnesota, USA, 2011. 9601, 9613
- Luhmann, A. J., Covington, M. D., Peters, A. J., Alexander, S. C., Anger, C. T., Green, J. A., Runkel, A. C., and Alexander Jr., E. C.: Classification of thermal patterns at karst springs and cave streams, *Ground Water*, 49, 324–335, 2011. 9591, 9592, 9615, 9621
- Luhmann, A. J., Covington, M. D., Alexander, S. C., Chai, S. Y., Schwartz, B. F., Groten, J. T., and Alexander Jr., E. C.: Comparing conservative and nonconservative tracers in karst and using them to estimate flow path geometry, *J. Hydrol.*, 448–449, 201–211, 2012. 9591, 9592, 9612, 9613, 9614, 9615, 9618, 9623
- Maillet, E. T.: *Essais d'Hydraulique Souterraine & Fluviale*, Hermann, Paris, 1905. 9591
- Markle, J. M. and Schincariol, R. A.: Thermal plume transport from sand and gravel pits – Potential thermal impacts on cool water streams, *J. Hydrol.*, 338, 174–195, 2007. 9591
- Martin, J. B. and Dean, R. W.: Temperature as a natural tracer of short residence times for groundwater in karst aquifers, in: *Karst Modeling*, Special Publication 5, edited by: Palmer, A. N., Palmer, M. V., and Sasowsky, I. D., Karst Waters Institute, Charles Town, West Virginia, USA, 236–242, 1999. 9591, 9592

**Thermal damping
and retardation in
karst conduits**

A. J. Luhmann et al.

[Title Page](#)[Abstract](#)[Introduction](#)[Conclusions](#)[References](#)[Tables](#)[Figures](#)[Back](#)[Close](#)[Full Screen / Esc](#)[Printer-friendly Version](#)[Interactive Discussion](#)

- Molson, J. W., Frind, E. O., and Palmer, C. D.: Thermal energy storage in an unconfined aquifer: 2. Model development, validation, and application, *Water Resour. Res.*, 28, 2857–2867, 1992. 9591
- Molson, J. W., Pehme, P., Cherry, J., and Parker, B.: Numerical analysis of heat transport within fractured sedimentary rock: Implications for temperature probes, in: Proceedings: NGWA/U.S. EPA Fractured Rock Conference: State of the Science and Measuring Success in Remediation, 24–26 September 2007, Portland, Maine, USA, 2007. 9591
- Newson, M. D.: A model of subterranean limestone erosion in the British Isles based on hydrology, *T. I. Brit. Geogr.*, 54, 55–70, 1971. 9591
- O'Driscoll, M. A. and DeWalle, D. R.: Stream–air temperature relations to classify stream–ground water interactions in a karst setting, central Pennsylvania, USA, *J. Hydrol.*, 329, 140–153, 2006. 9592
- Palmer, C. D., Blowes, D. W., Frind, E. O., and Molson, J. W.: Thermal energy storage in an unconfined aquifer: 1. Field injection experiment, *Water Resour. Res.*, 28, 2845–2856, 1992. 9591
- Raeisi, E., Groves, C., and Meiman, J.: Effects of partial and full pipe flow on hydrochemographs of Logsdon River, Mammoth Cave Kentucky USA, *J. Hydrol.*, 337, 1–10, 2007. 9620
- Renner, S.: Wärmetransport in Einzelklüften und Kluftaquiferen – Untersuchungen und Modellrechnungen am Beispiel eines Karstaquifers, Ph.D. thesis, Tübinger Geowissenschaftliche Arbeiten C30, University of Tübingen, Tübingen, Germany, 1996. 9591
- Ryan, M. and Meiman, J.: An examination of short-term variations in water quality at a karst spring in Kentucky, *Ground Water*, 34, 23–30, 1996. 9615
- Sauter, M.: Quantification and Forecasting of Regional Groundwater Flow and Transport in a Karst Aquifer (Gallusquelle, Malm, SW. Germany), Ph.D. thesis, Tübinger Geowissenschaftliche Arbeiten C13, University of Tübingen, Tübingen, Germany, 1992. 9615
- Screaton, E., Martin, J. B., Ginn, B., and Smith, L.: Conduit properties and karstification in the unconfined Floridan Aquifer, *Ground Water*, 42, 338–346, 2004. 9591, 9592
- Tallaksen, L. M.: A review of baseflow recession analysis, *J. Hydrol.*, 165, 349–370, 1995. 9591
- Ternan, J. L.: Comments on the use of a calcium hardness variability index in the study of carbonate aquifers: With reference to the Central Pennines, England, *J. Hydrol.*, 16, 317–321, 1972. 9591
- White, W. B.: Karst hydrology: Recent developments and open questions, *Eng. Geol.*, 65, 85–105, 2002. 9591

**Thermal damping
and retardation in
karst conduits**

A. J. Luhmann et al.

[Title Page](#)[Abstract](#)[Introduction](#)[Conclusions](#)[References](#)[Tables](#)[Figures](#)[⏪](#)[⏩](#)[◀](#)[▶](#)[Back](#)[Close](#)[Full Screen / Esc](#)[Printer-friendly Version](#)[Interactive Discussion](#)

- Worthington, S. R. H.: A comprehensive strategy for understanding flow in carbonate aquifers, in: Karst Modeling, Special Publication 5, edited by: Palmer, A. N., Palmer, M. V., and Sasowsky, I. D., Karst Waters Institute, Charles Town, West Virginia, USA, 30–37, 1999. 9590
- 5 Worthington, S. R. H., Davies, G. J., and Quinlan, J. F.: Geochemistry of springs in temperate carbonate aquifers: Recharge type explains most of the variation, in: Annales Scientifiques de l'Université de Besançon, Geologie–Mémoire Hors Série, edited by: Chauve, P. and Zwahlen, F., Cinquième Colloque d'Hydrologie en Pays Calcaire et en Milieu Fissuré, 16–18 October 1992, Neuchâtel, Switzerland, 11, 341–347, 1992. 9591
- 10 Worthington, S. R. H., Ford, D. C., and Beddows, P. A.: Porosity and permeability enhancement in unconfined carbonate aquifers as a result of dissolution, in: Speleogenesis: Evolution of Karst Aquifers, edited by: Klimchouk, A. V., Ford, D. C., Palmer, A. N., and Dreybrodt, W., National Speleological Society of America, Huntsville, Alabama, USA, 220–223, 2000. 9590

HESSD

11, 9589–9642, 2014

Thermal damping and retardation in karst conduits

A. J. Luhmann et al.

Title Page

Abstract

Introduction

Conclusions

References

Tables

Figures

⏪

⏩

⏴

⏵

Back

Close

Full Screen / Esc

Printer-friendly Version

Interactive Discussion



Table 1. Default parameters used in simulations.

Parameter	Value	Units
D_H	1	m
L	1000	m
V	0.626	m s^{-1}
\mathcal{R}_A	10	$^{\circ}\text{C}$
\mathcal{R}_D	60 000	s
k_r	2.15	$\text{W m}^{-1} ^{\circ}\text{C}^{-1}$
$c_{p,r}$	810	$\text{J kg}^{-1} ^{\circ}\text{C}^{-1}$
ρ_r	2320	kg m^{-3}
k_w	0.58	$\text{W m}^{-1} ^{\circ}\text{C}^{-1}$
$c_{p,w}$	4200	$\text{J kg}^{-1} ^{\circ}\text{C}^{-1}$
ρ_w	1000	kg m^{-3}
μ_w	1.3×10^{-3}	$\text{kg s}^{-1} \text{m}^{-1}$
D_L	0.01	$\text{m}^2 \text{s}^{-1}$
Pr	9.5	–

Thermal damping and retardation in karst conduits

A. J. Luhmann et al.

Table 2. Thermal transmission factors and retardation values of variable D_H and constant $D_{H,e}$ simulations.

D_H or $D_{H,E}$ (m)	L (m)	V (m s ⁻¹)	F (–)	τ (s)
1 and 1.2 1.11	2500 and 2500 4959	0.144 and 0.1 0.117	0.42 0.42	2220 2220
1 and 2 1.67	2500 and 2500 4500	0.4 and 0.1 0.144	0.65 0.65	1040 1050

Other parameters different from values in Table 1: $\mathcal{R}_D = 6000$ s.

[Title Page](#)
[Abstract](#)
[Introduction](#)
[Conclusions](#)
[References](#)
[Tables](#)
[Figures](#)
[Back](#)
[Close](#)
[Full Screen / Esc](#)
[Printer-friendly Version](#)
[Interactive Discussion](#)


Thermal damping and retardation in karst conduits

A. J. Luhmann et al.

Table 3. Thermal transmission factors and retardation values of variable V and equivalent constant V simulations.

V (m s^{-1})	\mathcal{R}_D (s)	L/V (s)	\mathcal{R}_D to L/V ratio	F (–)	τ (s)
variable (but more time at V below average V) 0.101	600	49,679	$\ll 1$	0.10	1470
	600	49 689	$\ll 1$	0.06	1360
variable (but more time at V below average V) 0.106	6000	46 806	< 1	0.43	3900
	6000	47 036	< 1	0.34	2800
variable (but more time at V below average V) 0.147	33 000	32 356	~ 1	0.70	5400
	33 000	33 902	~ 1	0.69	4700
variable (but more time at V above average V) 0.179	60 000	27 193	> 1	0.78	4700
	60 000	27 924	> 1	0.78	5200
variable (but more time at V above average V) 0.200	600 000	25 020	$\gg 1$	0.91	14 600
	600 000	25 050	$\gg 1$	0.91	15 400

Other parameters different from values in Table 1: $L = 5000$ m.

[Title Page](#)
[Abstract](#)
[Introduction](#)
[Conclusions](#)
[References](#)
[Tables](#)
[Figures](#)
[Back](#)
[Close](#)
[Full Screen / Esc](#)
[Printer-friendly Version](#)
[Interactive Discussion](#)


Thermal damping and retardation in karst conduits

A. J. Luhmann et al.

Table 4. Thermal transmission factors and retardation values of open channel simulations with different A_d/A_w ratios.

Channel type	\mathcal{R}_D (s)	A_w (-)	A_d (-)	F (-)	τ (s)
Full	6000			0.80	540
Full – cylindrical	6000			0.79	530
Mostly full	6000	3	1.4	0.79	540
Half full	6000	3	3	0.79	540
Mostly empty	6000	3	11	0.79	540
Full	60 000			0.93	1800
Full – cylindrical	60 000			0.92	1830
Mostly full	60 000	3	1.4	0.92	1850
Half full	60 000	3	3	0.92	1830
Mostly empty	60 000	3	11	0.92	1810
Full	600 000			0.98	5800
Full – cylindrical	600 000			0.96	6100
Mostly full	600 000	3	1.4	0.97	6600
Half full	600 000	3	3	0.97	6400
Mostly empty	600 000	3	11	0.96	6100

Other parameters different from values in Table 1: $V = 0.1 \text{ m s}^{-1}$.

Title Page

Abstract

Introduction

Conclusions

References

Tables

Figures



Back

Close

Full Screen / Esc

Printer-friendly Version

Interactive Discussion



Thermal damping and retardation in karst conduits

A. J. Luhmann et al.

Table 5. Thermal transmission factors and retardation values of different recharge shape simulations.

Thermograph shape	\mathcal{R}_D (s)	F (–)	τ (s)
Sine _H	6000	0.34	3220
Sine _O	6000	0.33	3090
Gaussian	6000	0.32	2960
Triangle	6000	0.31	3090
Sine _H	60 000	0.66	10 900
Sine _O	60 000	0.65	10 100
Gaussian	60 000	0.65	9300
Triangle	60 000	0.62	6500

Other parameters different from values in Table 1: $L = 5000$ m and $V = 0.1 \text{ m s}^{-1}$.

[Title Page](#)
[Abstract](#)
[Introduction](#)
[Conclusions](#)
[References](#)
[Tables](#)
[Figures](#)
[⏪](#)
[⏩](#)
[◀](#)
[▶](#)
[Back](#)
[Close](#)
[Full Screen / Esc](#)
[Printer-friendly Version](#)
[Interactive Discussion](#)


Table 6. Notation.

A_d	P_d/W_{fs} (unitless)
A_w	P_w/W_{fs} (unitless)
$c_{p,r}$	specific heat capacity of rock ($J\ kg^{-1}\ ^\circ C^{-1}$)
$c_{p,w}$	specific heat capacity of water ($J\ kg^{-1}\ ^\circ C^{-1}$)
C_{cyl}	correction factor for damping in cylindrical coordinates (unitless)
C_{time}	time conversion constant (unitless)
D_H	conduit hydraulic diameter (m)
$D_{H,avg}$	average conduit hydraulic diameter (m)
$D_{H,e}$	effective conduit hydraulic diameter (m)
$D_{H,i}$	conduit hydraulic diameter of segment i (m)
D_L	longitudinal dispersivity ($m^2\ s^{-1}$)
f	Darcy–Weisbach friction factor (unitless)
F	thermal transmission factor (unitless)
F_{cyl}	thermal transmission factor in cylindrical coordinates (unitless)
F_i	thermal transmission factor of segment i (unitless)
F_{planar}	thermal transmission factor in planar coordinates (unitless)
F_T	total thermal transmission factor for multisegment conduit system (unitless)
h_{conv}	water convection heat transfer coefficient ($W\ m^{-2}\ ^\circ C^{-1}$)
h_{rad}	radiation heat transfer coefficient ($W\ m^{-2}\ ^\circ C^{-1}$)
$H_i^{(1)}$	Hankel functions of the first kind
k_r	thermal conductivity of rock ($W\ m^{-1}\ ^\circ C^{-1}$)
k_w	thermal conductivity of water ($W\ m^{-1}\ ^\circ C^{-1}$)
L	conduit length (m)
L_e	effective conduit length (m)
L_i	length of conduit segment i (m)
Nu	Nusselt Number (unitless)
P_d	conduit dry perimeter (m)
P_w	conduit wetted perimeter (m)

Thermal damping and retardation in karst conduits

A. J. Luhmann et al.

[Title Page](#)

[Abstract](#) [Introduction](#)

[Conclusions](#) [References](#)

[Tables](#) [Figures](#)

[⏪](#) [⏩](#)

[◀](#) [▶](#)

[Back](#) [Close](#)

[Full Screen / Esc](#)

[Printer-friendly Version](#)

[Interactive Discussion](#)



Table 6. Continued.

Pe	longitudinal dispersion Peclet Number (unitless)
Pr	Prandtl Number (unitless)
r	radial distance from the conduit center into the surrounding rock (m)
R	conduit radius (m)
\mathcal{R}_A	recharge amplitude ($^{\circ}\text{C}$)
\mathcal{R}_D	recharge duration (s)
$\mathcal{R}_{D,Ex1}$	recharge duration during first pool trace experiment (s)
$\mathcal{R}_{D,Ex2}$	recharge duration during second pool trace experiment (s)
Re	Reynolds Number (unitless)
sine_H	half period of a sine function between two consecutive zeros (unitless)
sine_O	one period of a sine function from one trough to the next (unitless)
t	time (s)
t_{ft}	fluid flow-through time through the conduit, L/V (s)
$t_{ft,i}$	fluid flow-through time through segment i , L_i/V_i (s)
$t_{\text{peak,in}}$	temperature peak at conduit beginning ($x = 0$) ($^{\circ}\text{C}$)
$t_{\text{peak,out}}$	temperature peak at conduit end ($x = L$) ($^{\circ}\text{C}$)
T_r	rock temperature ($^{\circ}\text{C}$)
$T_{r,0}$	initial rock temperature ($^{\circ}\text{C}$)
$T_{r,\infty}$	rock temperature at an infinite distance from conduit axis ($^{\circ}\text{C}$)
$T_{r,d}$	dry rock temperature ($^{\circ}\text{C}$)
$T_{r,w}$	wet rock temperature ($^{\circ}\text{C}$)
T_r'	$T_r - T_{r,\infty}$ ($^{\circ}\text{C}$)
T_s	conduit surface temperature ($^{\circ}\text{C}$)
$T_{s,d}$	dry conduit surface temperature ($^{\circ}\text{C}$ or K)
$T_{s,w}$	wet conduit surface temperature ($^{\circ}\text{C}$)
T_w	water temperature ($^{\circ}\text{C}$ or K)
$T_{w,in}$	water temperature at conduit beginning ($x = 0$) ($^{\circ}\text{C}$)
$T_{w,in}'$	$T_{w,in} - T_{r,\infty}$ ($^{\circ}\text{C}$)
$T_{w,out}$	water temperature at conduit end ($x = L$) ($^{\circ}\text{C}$)
$T_{w,out}'$	$T_{w,out} - T_{r,\infty}$ ($^{\circ}\text{C}$)

Thermal damping and retardation in karst conduits

A. J. Luhmann et al.

Title Page

Abstract

Introduction

Conclusions

References

Tables

Figures

⏪

⏩

◀

▶

Back

Close

Full Screen / Esc

Printer-friendly Version

Interactive Discussion



Table 6. Continued.

$T_{w,peak,in}$	peak/trough water temperature at conduit beginning ($x = 0$) ($^{\circ}\text{C}$)
$T_{w,peak,out}$	peak/trough water temperature at conduit end ($x = L$) ($^{\circ}\text{C}$)
V	flow velocity in conduit (m s^{-1})
V_0	initial flow velocity in conduit (m s^{-1})
V_A	flow velocity amplitude (m s^{-1})
V_e	equivalent flow velocity in conduit (m s^{-1})
V_i	flow velocity in conduit of segment i (m s^{-1})
\bar{V}	average or reference flow velocity (m s^{-1})
W_{fs}	width of the water free surface (m)
x	longitudinal position along conduit (m)
y	distance from the conduit center into the surrounding rock (m)
α_r	thermal diffusivity of rock ($\text{m}^2 \text{s}^{-1}$)
ϵ	roughness height (m)
Θ	advection and conduction time ratio (unitless)
$\lambda_{T,sin}$	thermal length scale for sinusoidal temperature variations (m)
μ_w	dynamic viscosity of water ($\text{kg m}^{-1} \text{s}^{-1}$)
ρ_r	density of rock (kg m^{-3})
ρ_w	density of water (kg m^{-3})
σ	width of thermal Gaussian pulse (s)
σ_{SB}	Stefan-Boltzmann constant ($\text{W m}^{-2} \text{K}^{-4}$)
τ	retardation of thermal peak/trough (s)
τ_{Ex1}	retardation of thermal peak during first pool trace experiment (s)
τ_{Ex2}	retardation of thermal peak during second pool trace experiment (s)
τ_i	retardation of thermal peak/trough for segment i (s)
τ_{planar}	retardation of thermal peak/trough in planar coordinates (s)
τ_T	total retardation of thermal peak/trough for multisegment conduit system (s)
Ψ	$\rho_w c_{p,w} / (\rho_r c_{p,r})$ (unitless)
ω	angular frequency

Thermal damping and retardation in karst conduits

A. J. Luhmann et al.

[Title Page](#)

[Abstract](#) [Introduction](#)

[Conclusions](#) [References](#)

[Tables](#) [Figures](#)

[⏪](#) [⏩](#)

[◀](#) [▶](#)

[Back](#) [Close](#)

[Full Screen / Esc](#)

[Printer-friendly Version](#)

[Interactive Discussion](#)



Thermal damping and retardation in karst conduits

A. J. Luhmann et al.

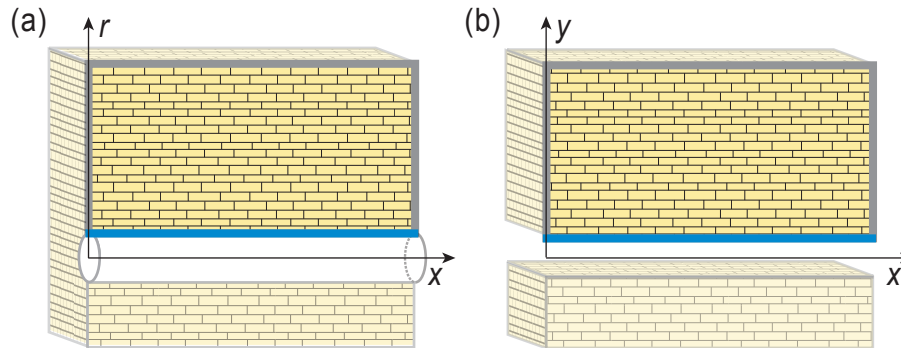


Figure 1. Model setup for heat transport simulations involving a **(a)** conduit or **(b)** fracture and the surrounding rock. The advection-dispersion equation is solved along the 1-D **(a)** conduit or **(b)** fracture. Because of symmetry, conduction in the 3-D rock surrounding the conduit or fracture may be modeled with a simple 2-D rectangle (outlined in thick gray and blue lines). Thus, conduction is modeled in **(a)** 2-D cylindrical or **(b)** 2-D planar coordinates. The two geometries are coupled to each other at each respective thick blue line (i.e., the conduit/fracture wall surface). Thick gray limestone boundaries perpendicular to the conduit or fracture are insulated rock boundaries. Thick gray limestone boundaries parallel to the conduit or fracture are sufficiently far from flow path lines to satisfy Eqs. (7) or (9), respectively, and are set to background temperature.

[Title Page](#)
[Abstract](#)
[Introduction](#)
[Conclusions](#)
[References](#)
[Tables](#)
[Figures](#)
[⏪](#)
[⏩](#)
[◀](#)
[▶](#)
[Back](#)
[Close](#)
[Full Screen / Esc](#)
[Printer-friendly Version](#)
[Interactive Discussion](#)


Thermal damping and retardation in karst conduits

A. J. Luhmann et al.

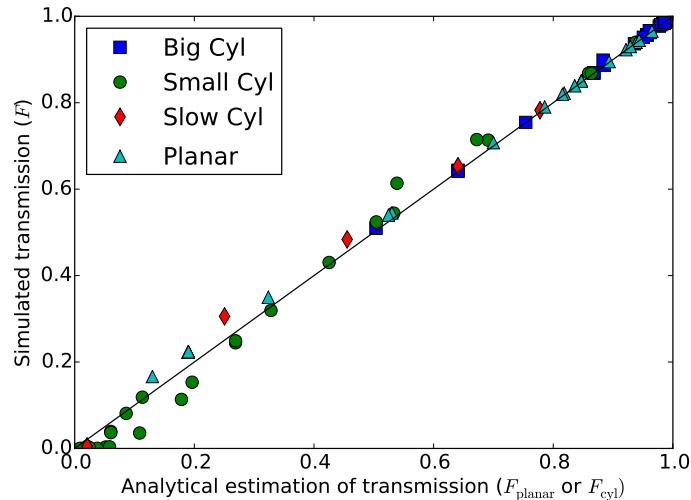


Figure 2. A comparison of the transmission factors of peaks in the simulations of Gaussian temperature pulses against the modified form of the analytical solution for a sinusoidal input temperature (Eq. 36). Cylindrical cases are corrected by an additional factor (Eq. 37) that is a function of the dimensionless parameter Θ . These modified forms of the analytical solution provide a close fit to the simulation results for most cases. Big Cyl and Small Cyl indicate a conduit in cylindrical coordinates with a $D_H \geq 1$ m and a $D_H < 1$ m, respectively. Slow Cyl indicates a conduit in cylindrical coordinates with a $V \leq 0.0352$ m s⁻¹. Planar indicates a conduit in planar coordinates.

Title Page

Abstract

Introduction

Conclusions

References

Tables

Figures

⏪

⏩

◀

▶

Back

Close

Full Screen / Esc

Printer-friendly Version

Interactive Discussion



**Thermal damping
and retardation in
karst conduits**

A. J. Luhmann et al.

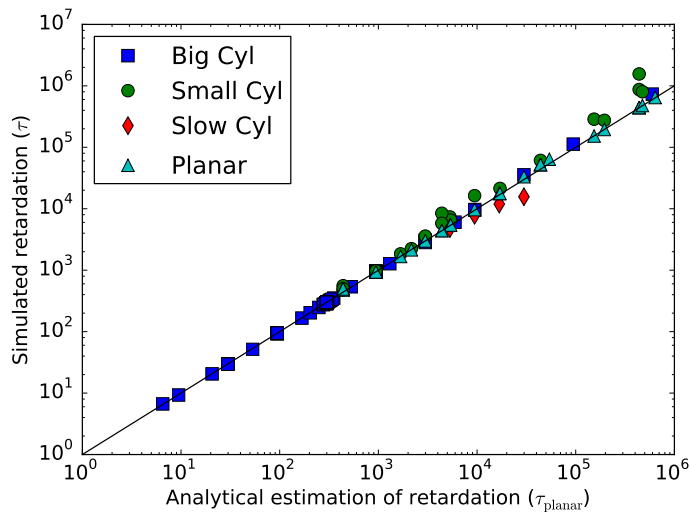


Figure 3. Simulated retardation as a function of theoretical retardation. In general, there is excellent agreement between the analytical solution and numerical simulations. Legend categories are the same as Fig. 2.

[Title Page](#)[Abstract](#)[Introduction](#)[Conclusions](#)[References](#)[Tables](#)[Figures](#)[Back](#)[Close](#)[Full Screen / Esc](#)[Printer-friendly Version](#)[Interactive Discussion](#)

Thermal damping and retardation in karst conduits

A. J. Luhmann et al.

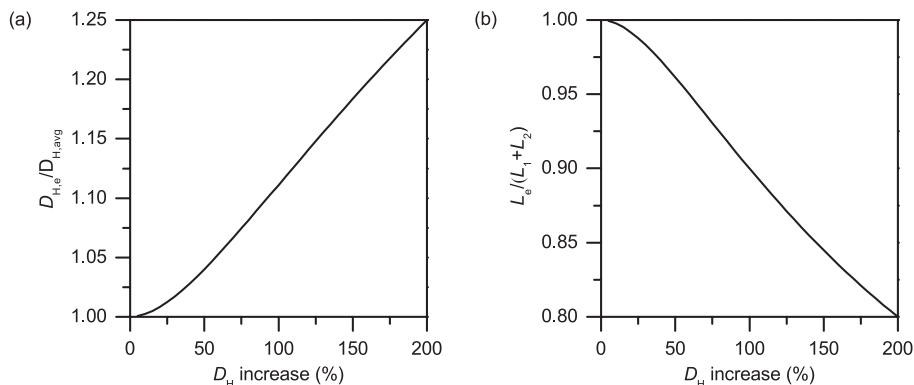


Figure 4. (a) $D_{H,e}/D_{H,avg}$ and (b) $L_e/(L_1+L_2)$ for different relative increases in D_H when $L_1 = L_2$. The $D_{H,e}$ for a flow path with two sections of different D_H is generally more heavily weighted toward the section with a larger D_H , and a larger increase in D_H produces a larger $D_{H,e}$. The L_e for a flow path with two sections of different D_H is always less than $L_1 + L_2$, and a larger increase in D_H results in a smaller L_e .

[Title Page](#)
[Abstract](#)
[Introduction](#)
[Conclusions](#)
[References](#)
[Tables](#)
[Figures](#)

[Back](#)
[Close](#)
[Full Screen / Esc](#)
[Printer-friendly Version](#)
[Interactive Discussion](#)


**Thermal damping
and retardation in
karst conduits**

A. J. Luhmann et al.

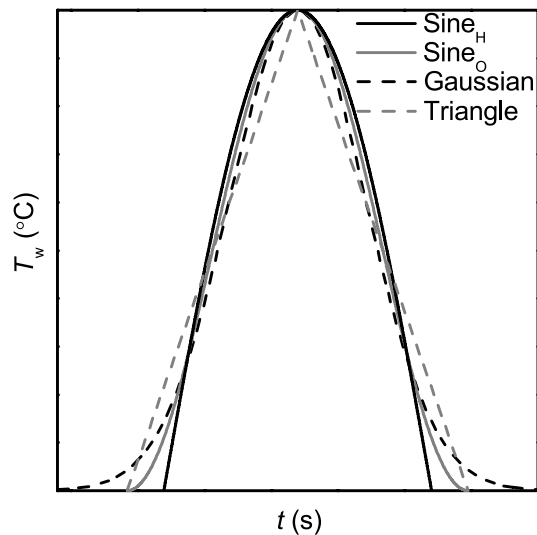


Figure 5. Different modeled recharge shapes. The sine_H curve is widest near the peak and produces less damping and more retardation than the other recharge shapes. Note the ends of the Gaussian curve are not shown in this figure.

[Title Page](#)[Abstract](#)[Introduction](#)[Conclusions](#)[References](#)[Tables](#)[Figures](#)[◀](#)[▶](#)[◀](#)[▶](#)[Back](#)[Close](#)[Full Screen / Esc](#)[Printer-friendly Version](#)[Interactive Discussion](#)

Thermal damping
and retardation in
karst conduits

A. J. Luhmann et al.

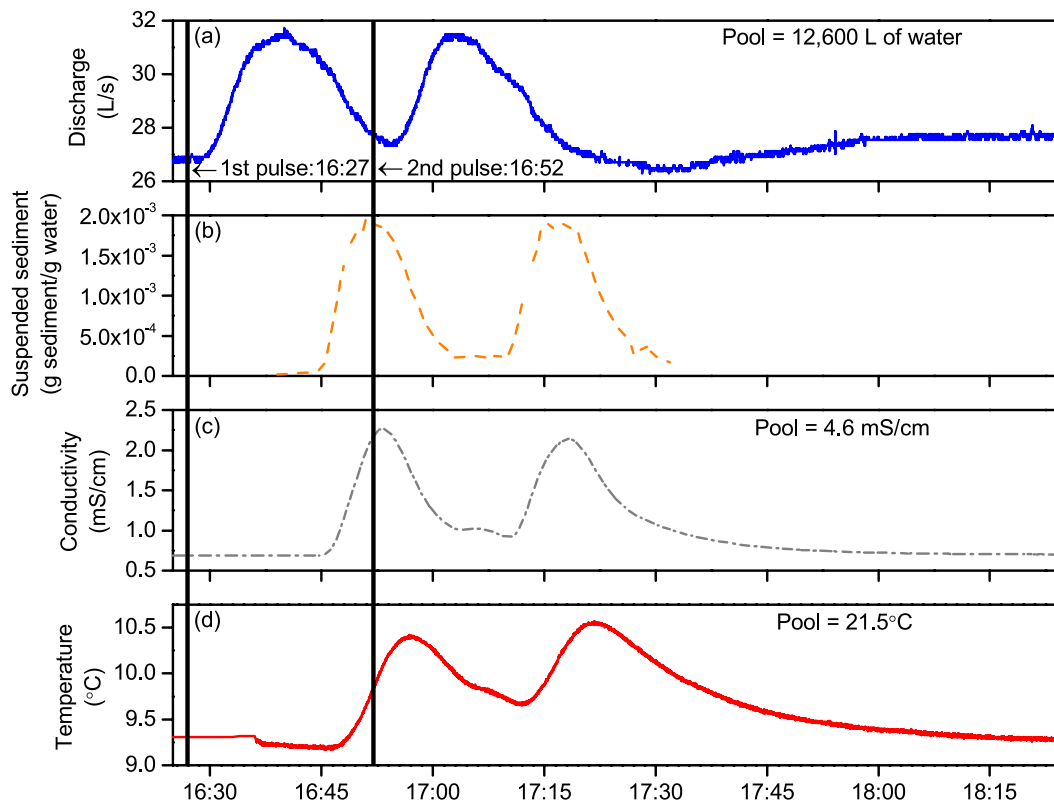


Figure 6. (a) Discharge, (b) suspended sediment, (c) electrical conductivity, and (d) temperature breakthrough curves at Freiheit Spring on 2 September 2010. Water was added to a pool at the edge of a sinkhole, and the water was heated as salt was added. The water was emptied into the sinkhole, and breakthrough curves were monitored at Freiheit Spring approximately 95 m away.

[Title Page](#)[Abstract](#)[Introduction](#)[Conclusions](#)[References](#)[Tables](#)[Figures](#)[◀](#)[▶](#)[◀](#)[▶](#)[Back](#)[Close](#)[Full Screen / Esc](#)[Printer-friendly Version](#)[Interactive Discussion](#)